Does a dysfunctional heart alter excitatory synapses in the hippocampus?

Øyvind Pernell Haugen

Thesis for the Master's degree in Molecular Biosciences

Department of Biosciences
Faculty of Mathematics and Natural Sciences

UNIVERSITY OF OSLO

June 2014

Does a dysfunctional heart alter excitatory synapses in the hippocampus?

Master's degree
60 study points

Department of Biosciences
Faculty of Mathematics and Natural Sciences

UNIVERSITY OF OSLO

June 2014

2014

Does a dysfunctional heart alter excitatory synapses in the hippocampus?

Supervisors: Linda Hildegard Bergersen, Marianne Fyhn

http://www.duo.uio.no/

Trykk: Reprosentralen, Universitetet i Oslo

Abstract

It is known that elderly people suffering from heart disease can have memory problems. The hippocampus is the part of the brain that is essential for memory formation and is one of the areas that is most vulnerable to cerebral hypoperfusion. Long-term potentiation is widely accepted as the cellular basis for memory. Upregulation of glutamate receptors of the α-amino-3-hydroxy-5-methyl-4-isoxazolepropionic acid (AMPA) and N-methyl-D-aspartate (NMDA) type in the synaptic membranes is important to make the synapses more efficient during long-term potentiation. While animal models of acute global or focal brain ischemia have been widely investigated, the brain effects caused by a dysfunctional heart have been insufficiently studied, in particular with respect to cellular and molecular mechanisms that link heart failure to cognitive impairment.

To address the issue of a relation between heart failure and cognitive impairment, we have used a mouse model with specific, inducible expression of the mutUNG1enzyme in the heart. The mutUNG1 enzyme generates mitochondrial DNA damage in the form of apurinic/apyrimidinic sites which leads to mitochondrial impairment in cardiomyocytes and ultimately a dysfunctional heart. This gives the opportunity to study possible changes in the brain of a chronic heart failure mouse model. The aim of this thesis was to investigate whether a dysfunctional heart affects the expression of AMPA and NMDA receptors in the hippocampus, which would provide a possible explanation to the memory deficits experienced by patients suffering from heart disease.

Quantitative polymerase chain reaction was used to quantify the gene expression of AMPA and NMDA receptors. Quantitative electron microscopy, by the use of postembedding immunogold labelling, was used to study the number of AMPA and NMDA receptors present in excitatory synapses of the hippocampus, as well as synaptic morphology in the form of postsynaptic density length.

The results obtained by qPCR showed large variations in gene expression within both groups, but no significant difference was found between them. Quantitative electron microscopy

showed no significant differences in number of receptors at the protein level and in the length of postsynaptic densities.

These results show that acute heart failure as induced in this mouse model may not be sufficient to have an impact on the brain. Nonetheless, the use of a different chronic heart failure model in future studies could show a link between heart failure and cognitive decline.

Acknowledgements

The work presented in this thesis was carried out at the Brain and Muscle Energy group & Synaptic Neurochemistry Laboratory, Department of Anatomy, Institute of Basic Medical Sciences, University of Oslo.

First and foremost, I would like to thank my principal supervisor Professor Linda Hildegard Bergersen for giving me the opportunity to work on this exciting project and for the helpful guidance. Her knowledge and enthusiasm in the field of neurobiology have been a great inspiration. I would also like to thank my internal supervisor at the Institute of Biosciences, UiO, Professor Marianne Fyhn, for support and constructive discussion.

Thanks are also due to my co-supervisor Knut Husø Lauritzen for the opportunity to work with his mouse model, for helping me out in the lab and for always welcoming me and being helpful when support was needed. The same goes for Liv Kleppa, Maja Puchades and Christine Regnell – without you, I would not have been able to complete my project.

I would like to express my gratitude to all the members of the lab for contributing to the friendly and good working environment.

A special thanks to Mari Kaarbø, Oslo University Hospital, for sharing her endless knowledge about qPCR with me.

Last, but not least; thanks to my family and friends for all the encouragement and support.

Abbreviations

AMPA	α-amino-3-hydroxy-5-methyl-4-isoxazolepropionic acid
ATP	Adenosine triphosphate
BER	Base excision repair
bp	Base pair
BSA	Bovine serum albumin
CA	Cornu ammonis (hippocampal subfields 1-3)
CaMKII	Ca^{2+}/calmodulin-dependent protein kinase II
DNA	Deoxyribonucleic acid
DNase	Deoxyribonuclease
Dox	Doxycycline
dsDNA	Double-stranded DNA
DTT	Dithiothreitol
ECL	Enhanced chemiluminescence
EPSP	Excitatory postsynaptic potential
EtBr	Ethidium bromide
g	Gravitational acceleration
GAPDH	Glyceraldehyde 3-phosphate dehydrogenase
HF	Heart failure
HSA	Human serum albumin
IgG	Immunoglobulin G
IPSP	Inhibitory postsynaptic potential
Kb	Kilobases
kDA	Kilodalton
LTD	Long-term depression
LTP	Long-term potentiation
M	Mol/L
MHCα	Myosin heavy chain α (heart specific)
Min	Minutes
MQ water	Milli-Q water
mRNA	Messenger RNA
mtDNA	Mitochondrial DNA
nm	Nanometer
NMDA	N-methyl-D-aspartate
OD	Optical density
PB	Phosphate buffer
PEG	Polyethylene glycol
PSD	Postsynaptic density
qPCR	Quantitative polymerase chain reaction
RNA	Ribonucleic acid
RNase	Ribonuclease
Rpm	Rotations per minute
rtTA	Reverse tetracycline transactivator
RT-PCR	Reverse transcription polymerase chain reaction
SDS	Sodium dodecyl sulfate
SDS-PAGE	Sodium dodecyl sulfate polyacrylamide gel electrophoresis
TAE	Tris-acetate-ethylenediaminetetraacetic acid
TBST	Tris-buffered saline with Triton or Tween

Tet-on	tetracycline-controlled transcriptional activator turned on by tetracycline
UNG	Uracil-DNA glycosylase
UV	Ultraviolet light
WT	Wild type
°C	Degrees Celcius
µL	Microliter
µm	Micrometer

Figures

Illustrations are drawn by the author of this thesis unless otherwise stated.

Innholdsfortegnelse

1 Introduction

1.1 Effects of heart failure on cognitive function

The heart is pumping blood out to the whole body, supplying all the cells with nutrients and oxygen. It consists of muscle cells called cardiomyocytes which make the heart contract approximately 100 000 times per day. Apart from the heart, the brain is the organ with the highest blood supply. 15-20% of cardiac output goes to the brain, indicating the great need for glucose and oxygen required to maintain neuronal metabolism. Too low cerebral blood flow results in ischemia, rapidly leading to cell damage or cell death.

Heart failure (HF), i.e. the heart's pumping power is weaker than normal, is an increasing health problem that affects 1-2% of the global population and increases dramatically when surpassing the age of 65 (Dardiotis et al., 2012). HF has been shown to affect several cognitive abilities like attention, learning ability, memory, language, visuospatial function, executive function and psychomotor speed (Vogels et al., 2007a, 2007b). More than 40% of patients who underwent coronary artery bypass experience cognitive decline that continues after five years (Newman et al., 2001). There is also an ongoing debate on whether Alzheimer's disease is a neurodegenerative or cardiovascular disease, or a combination of both (de la Torre, 2004; Lee et al., 2014). Many of the cognitive functions, especially memory and learning, are related to the hippocampus, which has been shown to be vulnerable to ischemia (Schmidt-Kastner and Freund, 1991; Zhu et al., 2012). Since there seems to be a link between HF and cognitive decline, a great effort has recently been undertaken trying to uncover the underlying mechanisms.

1.2 Neurons

Neurons are one of the two primary cell types that constitute the nervous system, the other being glial cells. While the primary function of neurons is to transmit electrical signals, glial cells possess more diverse roles, like initiating immune responses (microglia), enhancing the electrical signals of neurons (oligodendrocytes) and regulating the chemical content of the

extracellular environment (astrocytes). A classical neuron consists of a dendritic tree, the soma and an axon (figure 1.1). Neurons are electrically excitable and connect to each other through specialized structures called synapses, allowing them to communicate. A synapse is typically located between a presynaptic axon terminal and a postsynaptic dendritic spine and is the release site for neurotransmitters. Different kinds of neurotransmitters can affect the postsynaptic neuron in different ways. Neurotransmitters that make the postsynaptic neuron more likely to generate electrical signals are said to be excitatory, whereas neurotransmitters that make postsynaptic neuron less likely to genereate electrical signals are said to be inhibitory. The effect is not dependent on the neurotransmitter itself, but on the type of receptor it binds to. Simple neurotransmitters, like single amino acids, are synthesized in the axon terminals, while larger neurotransmitters, like peptides and proteins, are synthesized in the soma and transported in vesicles all the way to the axon terminal.

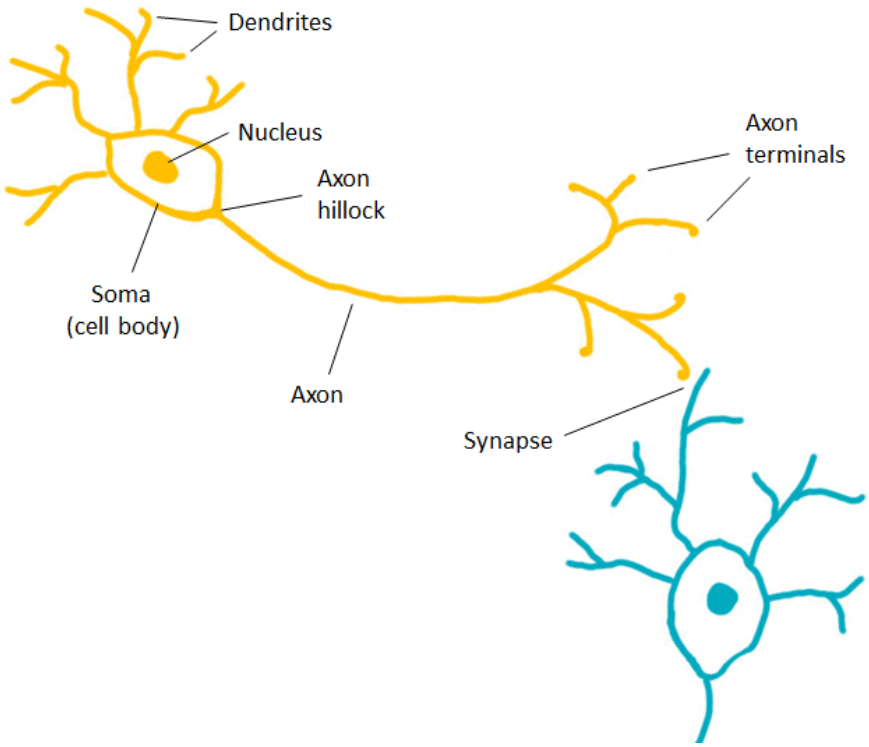

Figure 1.1 Illustration of neuron structure. A presynaptic neuron (yellow) and a postsynaptic neuron (blue) are shown. Action potentials are generated at the border between the soma and axon, at the axon hillock, from where it propagates down the axon until it reaches the axon terminal. Neurotransmitters are then released from the axon terminal, into the synaptic cleft, and bind to neurotransmitter receptors on the dendritic spine of the postsynaptic neuron. Depending on the type of receptor, the affect can either be excitatory or inhibitory.

1.3 The chemical synapse

The chemical synapse is a special membrane junction for neuronal communication. It consists of three components (figure 1.2):

1) The presynaptic membrane, which is part of the axon terminal and site for neurotransmitter release.
2) The synaptic cleft, which is the space between the pre- and postsynaptic neurons where neurotransmitters are released into.
3) The postsynaptic membrane, which is located on one of the dendrites of the postsynaptic neuron and contains neurotransmitter receptors.

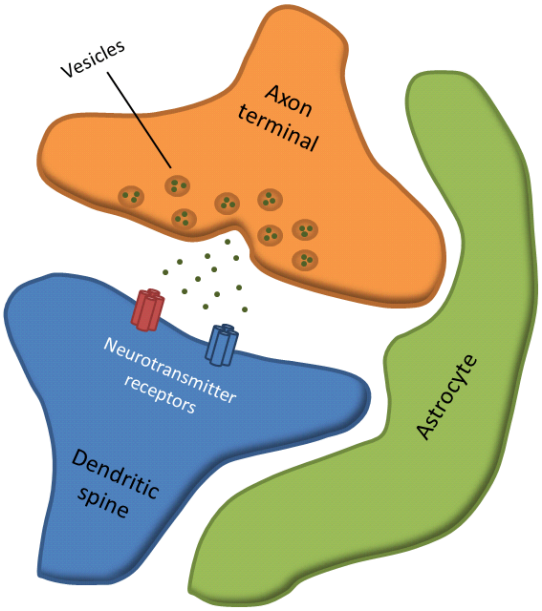

Figure 1.2 Illustration of a chemical synapse. These synapses are often encompassed by astrocytes, which regulate several aspects of the synapse, i.e. ion and water homeostasis and neurotransmitter uptake. The width of the synaptic cleft is approximately 20 nm.

Neurotransmitters are stored in vesicles located in the axon terminal, near the presynaptic membrane. When released into the synaptic cleft by exocytosis, the neurotransmitters will bind to receptors on the postsynaptic membrane in an area called the postsynaptic density (PSD) due to the many densely packed receptors and associated proteins located there.

Depending on the type of receptor, the binding of transmitter can initiate an excitatory postsynaptic potential (EPSP) or an inhibitory postsynaptic potential (IPSP). In this way, the electrical signal in the presynaptic neuron is transformed into a chemical signal that can either promote or prevent the postsynaptic neuron from generating a new electrical signal. The strength of the signal is determined by the amount of transmitter released, the density of the receptors and the rate of diffusion of the transmitter out of the synaptic cleft, which is governed by the activity of inactivating transporters. Simple neurotransmitters, like single amino acids, are recycled from the synaptic cleft by transportation into astrocytes and back to the neurons or by direct uptake into presynaptic terminals, whereas larger peptides and proteins are degraded by proteases.

1.4 Glutamate

In addition to being an important amino acid for protein synthesis, glutamate is the most abundant neurotransmitter in the brain. Nearly all excitatory synapses in the brain are glutamatergic. After release into the synaptic cleft, the glutamate has to be removed. Prolonged exposure to glutamate may initiate neuronal cell death by necrosis or apoptosis due to excessive influx of Ca^{2+}, a phenomena termed excitotoxicity (Ankarcrona et al., 1995; Arundine and Tymianski, 2003). The glutamate can be removed by the synaptic cleft by direct reuptake into the presynaptic terminal for reuse as neurotransmitters or transported into the postsynaptic dendrite (Gundersen et al., 1993; Takahashi et al., 1996). However, most of the glutamate is taken up by astrocytes where it is converted to glutamine (Laake et al., 1995). The amino acid glutamine is released into the extracellular space and subsequently transported into the presynaptic terminal where it is converted back to glutamate. This glutamate-glutamine cycle contributes to prevent the neurons from depleting their glutamate storage. Once inside the presynaptic terminal, the glutamate is transported into vesicles ready for another round of exocytosis (Naito and Ueda, 1983).

1.5 Glutamate receptors

Glutamate receptors are divided into two types: ionotropic and metabotropic. Whereas the latter are G-protein coupled receptors and operates through second messengers, the ionotropic

receptors form cation channels. The ionotropic glutamate receptors are divided into three families based on their selective agonists which mimic the effect of glutamate binding: α-Amino-3-hydroxy-5-methyl-4-isoxazolepropionic acid (AMPA), N-methyl-D-Aspartate (NMDA) and kainate receptors (table 1.1). They are heteromeric assemblies of four subunits (figure 1.3), each affecting the biophysical properties of the receptor (Traynelis et al., 2010).

Receptor family	**Subunit**	**Gene**
AMPA	GluA1	*GRIA1*
	GluA2	*GRIA2*
	GluA3	*GRIA3*
	GluA4	*GRIA4*
NMDA	NR1	*GRIN1*
	NR2A	*GRIN2A*
	NR2B	*GRIN2B*
	NR2C	*GRIN2C*
	NR2D	*GRIN2D*
	NR3A	*GRIN3A*
	NR3B	*GRIN3B*
Kainate	GluK1	*GRIK1*
	GluK2	*GRIK2*
	GluK3	*GRIK3*
	GluK4	*GRIK4*
	GluK5	*GRIK5*

Table 1.1 The different glutamate receptors and their subunits.

There are four AMPA receptor subunits: GluA1, GluA2, GluA3 and GluA4. AMPA receptors are diheteromeric, usually consisting of two GluA2 subunits and two of a different subunit. The ion channel of the receptor opens and closes quickly and has high permeability to Na^+, thus rapidly depolarizing the neuron. Due to the fast kinetic properties, AMPA receptors allow for high temporal precision and short latency of action potential initiation (Andersen et al., 2007, p. 251). The primary transcript of GluA2 undergoes RNA editing of a single glutamine to arginine (Sommer et al., 1991). This editing takes place in the pore-loop segment

and makes the AMPA receptor impermeable to Ca^{2+}, a property important for the regulation of synaptic plasticity like long-term potentiation (LTP) and long-term depression (LTD).

In addition to Na^{+}, NMDA receptors are permeable to Ca^{2+}. Ca^{2+} is an important second messenger that can initiate synaptic changes when entering the postsynaptic dendrite. Binding of glutamate alone is not sufficient to activate the NMDA receptor, as this also requires binding of glycine and a partial depolarization of the postsynaptic membrane. At resting potential, when the neuron does not receive input from other neurons, the cation channel of the NMDA receptor has a voltage-dependent Mg^{2+} block. A partial depolarization of the membrane, obtained by the activation of AMPA receptors, is required to repel the Mg^{2+} ion. The NMDA receptors are therefore said to function as coincidence detectors, as they will only open when several input signals are received closely in time (Seeburg et al., 1995). Compared to AMPA receptors, NMDA receptors have higher affinity for glutamate, slower activation kinetics and stay open for a longer time. There are seven NMDA receptor subunits: NR1, NR2A, NR2B, NR2C, NR2D, NR3A and NR3B. The NMDA receptors are predominantly diheteromeric, consisting of two NR1 subunits and two identical NR2 subunits. However, triheteromeric receptors are also expressed in certain brain areas, like the hippocampus (Tovar et al., 2013). The NR1 subunit is crucial for the NMDA receptor to function, as this subunit contains the binding site for glycine, and all NMDA receptors contain two of them. The NR2 subunits contain the binding site for glutamate. The diversity of NR2 subunits gives rise to different NMDA receptors, each having unique biophysical properties (Cull-Candy and Leszkiewicz, 2004). The NR2B subunit, for instance, has slower decay kinetics than the NR2A subunit and will therefore cause the channel to stay open longer. The distribution of NMDA receptor subunits is not constant, as the ratio of NR2 subunits has been shown to change in developing brain areas (Monyer et al., 1994). The NR3 subunits contain binding site for glycine, and NMDA receptors assembled from NR1 and NR3 subunits are activated by glycine only and are therefore not considered as glutamate receptor (Andersen et al., 2007, p. 253).

Less is known about the functional role of kainate receptors, which are located in other subcellular compartments in addition to the PSD. While AMPA and NMDA receptors

mediate most of the basal excitatory transmission, kainate receptors possess more diverse roles depending on their subunit composition and cellular localization (Carta et al., 2014). The EPSPs generated by kainate receptors are generally smaller compared to the EPSPs generated by AMPA receptors.

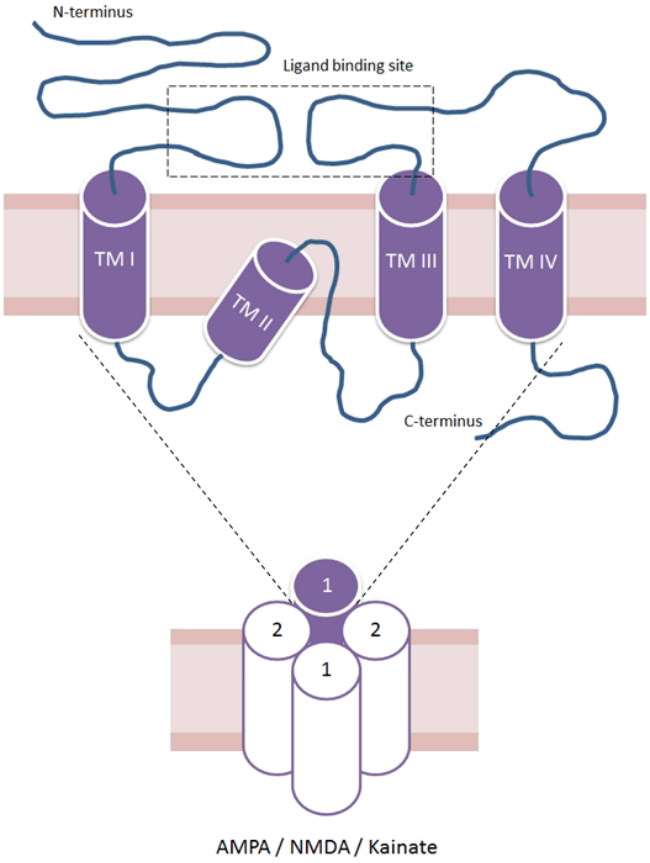

Figure 1.3 Structure of an ionotropic glutamate receptor and its subunits. The receptor subunit has four transmembrane domains (TM I-IV). The N-terminus is extracellular, while the C-terminus is intracellular because of the second transmembrane domain not fully traversing the membrane. The ligand binding site is located between the N-terminal loop and the loop connecting transmembrane domains III and IV. Most ionotropic glutamate receptors are diheteromeric assemblies of four subunits.

1.6 NMDA receptor-dependent LTP and LTD

Long-term potentiation (LTP) and long-term depression (LTD), two forms of synaptic plasticity, are thought to be the cellular mechanisms behind learning and memory. Different

types of LTP and LTD exist, but those occurring in the Schaffer collateral pathway of the hippocampus are classified as NMDA receptor-dependent and are the most studied form (Lüscher and Malenka, 2012). While both LTP and LTD require the influx of Ca^{2+} through NMDA receptors, the distinguishing factor seems to be the degree of influx. A large increase in intracellular Ca^{2+} promotes LTP, while a small increase promotes LTD.

Several methods to induce LTP and LTD have been used, e.g. frequency-specific presynaptic firing patterns and spike-timing-dependent plasticity (Lüscher and Malenka, 2012). The exact mechanisms during learning and memory formation in the intact animal are not fully understood. Nonetheless, LTP and LTD exhibit properties important for the formation of memories such as input specificity, associativity and cooperativity (Kandel et al., 2012).

LTP is dependent on the activation of Ca^{2+}-dependent protein kinases (figure 1.4a). Ca^{2+}/calmodulin-dependent kinase II (CaMKII) possesses a central role, as this kinase is known to phosphorylate AMPA receptors (Derkach et al., 1999), thereby enhancing their conductance, and is also needed for the insertion of additional AMPA receptors in the postsynaptic membrane (Hayashi et al., 2000). These mechanisms lead to strengthening of the synapse and thereby results in enhanced signal transmission between the neurons. The duration of LTP varies from seconds to months or longer (Abraham et al., 2002). The early phase of LTP is maintained by protein kinases, while the late phase requires synthesis of new proteins, either through translation of pre-existing mRNA located in the postsynaptic spine or by gene transcription (Abraham and Williams, 2003).

LTD, on the other hand, is dependent on protein phosphatases, which reverse the effect by dephosphorylating the AMPA receptors and promoting receptor endocytosis (figure 1.4b). It has been shown that two phosphatases involved in LTD, calcineurin and protein phosphatase 1 (PP1), have higher Ca^{2+} affinity than CaMKII (Lisman, 1989), which provides an explanation for the different Ca^{2+} levels required for LTP and LTD.

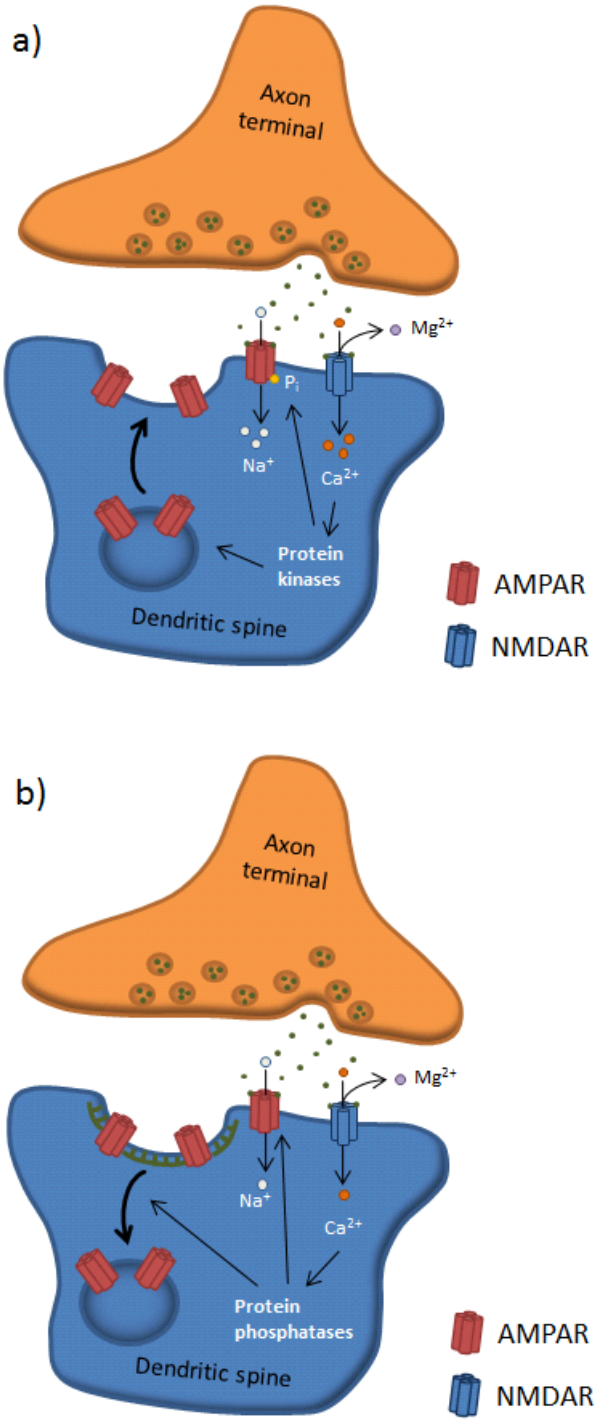

Figure 1.4 Schematic drawing of: a) NMDA receptor-dependent LTP. A rapid increase of Ca^{2+} leads to activation of protein kinases. This results in enhanced AMPA receptor conductivity and insertion of AMPA receptors into the postsynaptic membrane. Only the early phase of LTP is included in the drawing. b) NMDA receptor-dependent LTD. A slow increase in Ca^{2+} activates protein phosphatases. This leads to the reversal of the effects underlying LTP.

1.7 The hippocampus

The hippocampus is canonical model for the study of communication between neurons due to its intrinsic neural circuit. Most of the research regarding long-term potentiation (LTP) has been carried out in the hippocampus. Its main function is thought to be that of memory consolidation and spatial navigation. The hippocampus is part of the hippocampal formation and is located in the medial temporal lobe, one in each hemisphere. It consists of a tightly packed layer of pyramidal neurons that projects through three subfields termed CA3, CA2 and CA1 (Andersen et al., 2007, p. 37). In addition, there are many different inhibitory neurons that regulate the activity of the pyramidal neurons. The subfields are further divided into different layers, or strata, depending on where the different projections connect along the dendritric tree.

1.8 Hippocampal function: memory and spatial navigation

The hippocampus is required for the formation of declarative memories. Declarative memory can be divided into episodic memory and semantic memory (Tulving, 1972). Episodic memory is the recollection of events from an individual's own life where contextual factors like place and time are central. Semantic memory is general knowledge, or facts, about the world. Damage to the hippocampus indicates that its function is to consolidate this declarative memory for permanent storage in other cortical areas (Eichenbaum, 2013). Supporting this view is the observation of descending activity in the hippocampus when subjects try to recall more and more remote memories (Smith and Squire, 2009). The surgical removal of two thirds of each of the hippocampi in patient H.M. was the first case that proved the link between this brain area and its function to memory (Scoville and Milner, 1957). H.M. could not form new episodic or semantic memories after the surgery, but could form non-declarative (non-conscious) memories like motor skills, meaning that this type of memory is not dependent on the hippocampus. He did also show normal “working memory”, which is the ability to hold multiple pieces of information in mind while focused. However, several studies have now shown that the hippocampus is involved in working memory as well (Axmacher et al., 2009; Ben-Yakov and Dudai, 2011).

Hippocampus is also crucial for spatial navigation. The pyramidal neurons of the hippocampus function as «place cells», whose activity depend on specific locations in an environment. Together with other evidence, this observation led to the assumption that hippocampus functions as a cognitive map (O'Keefe and Nadel, 1978). The place cells receive input from other types of neurons in the hippocampal formation, e.g. the «grid cells» in the enthorinal cortex, which fire in a fixed grid like pattern, independent of the environment, when the rat is moving around (Hafting et al., 2005). The place fields of the hippocampus have been speculated to contribute with a context of space to episodic memories, e.g. where a particular event took place (Smith and Mizumori, 2006).

The role of the NMDA receptor has been strongly linked to all these properties, suggesting LTP and LTD as the cellular basis. Knockout of the NR1 subunit in CA1 pyramidal neurons in mice results in larger and more diffuce place fields, as well as uncorrelated activity (McHugh et al., 1996). Furthermore, blockage of NMDA receptors disrupted the long-term stability of place fields (Kentros et al., 1998). Upregulation of the NR2B subunit in hippocampus of transgenic mice enhanced LTP in the Schaffer collateral pathway because NR2B contributes to a longer opening time of NMDA receptors (Tang et al., 1999). The transgenic mice performed better at object recognition tasks, fear conditioning and the Morris water maze, which is a test used to study spatial learning and memory in rodents.

1.9 Intrinsic circuit of the hippocampus

The intrinsic circuit of the hippocampus is illustrated in figure 1.5. Axons from the enthorinal cortex project to the granule cell layer of the dentate gyrus. The mossy fibers of the granule cells project to the CA3 pyramidal neurons of the hippocampus, which in turn transmit signals through their Schaffer collateral fibers to CA1 pyramidal neurons. CA1 pyramidal neurons project to the subiculum and enthorinal cortex, thus enclosing the circuit and establishing what can be considered as a synaptic loop. Additionally, both CA3 and CA1 pyramidal neurons receive input directly from the enthorinal cortex, and CA3 has an associational/recurrent connection where axons project back to the CA3 subfield.

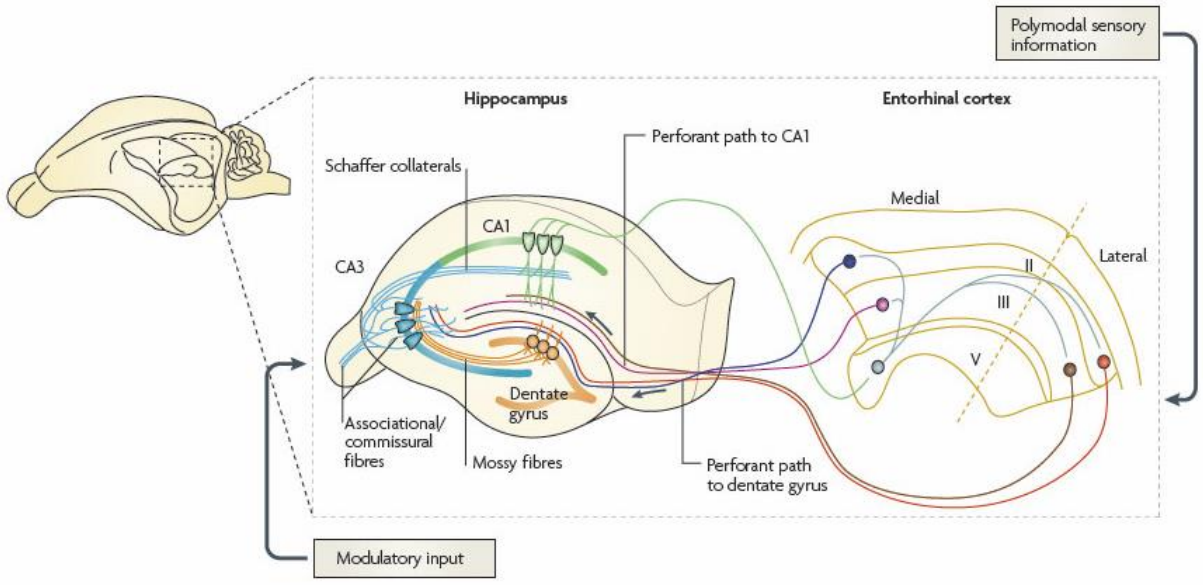

Figure 1.5 A schematic drawing of the intrinsic circuit of the hippocampal formation. The hippocampal formation includes the dentate gyrus, the hippocampus, the subicular complex and the enthorinal cortex (Andersen et al., 2007, p. 37). The subicular complex, consisting of the subiculum, presubiculum and parasubiculum, is not depicted here. It is located between the CA1 area and enthorinal cortex and is the the major extrinsic pathway out of the hippocampal formation to other cortical and subcortical areas. Figure from Neves et al., 2008.

1.10 The Schaffer collateral pathway

The pyramidal neurons of the CA1 subfield are slightly smaller than other pyramidal neurons. They are also more homogenous, as the size of the cell somas and length of the dendritic trees do not differ significantly (Andersen et al., 2007, p. 68). The axons traverse apical to the somas in an area called the alveus.

The major input to CA1 comes from CA3 and is termed the Schaffer collateral pathway. The Schaffer collaterals are axons from CA3 pyramidal neurons and project into the stratum radiatum of CA1, which is the layer right next to the pyramidal cell somas on the apical side. Here, the apical dendrites can be seen as thick stem dendrites with a lot of glutamatergic synapses connected to their spines (figure 1.6).

Most of the Schaffer collateral-CA1 synapses contain both AMPA and NMDA receptors. However, some contain only NMDA receptors and do not respond to incoming signals from

presynaptic terminals under normal conditions (Isaac et al., 1995). They are therefore termed «silent synapses». The number of silent synapses decreases with age, and LTP is thought to be the mechanism for «unsilencing» these synapses by insertion of AMPA receptors. It has also been shown that the PSD of silent synapses has a shorter diameter compared to the PSD of synapses containing NMDA receptors, which may be due to the lack of AMPA receptors (Takumi et al., 1999).

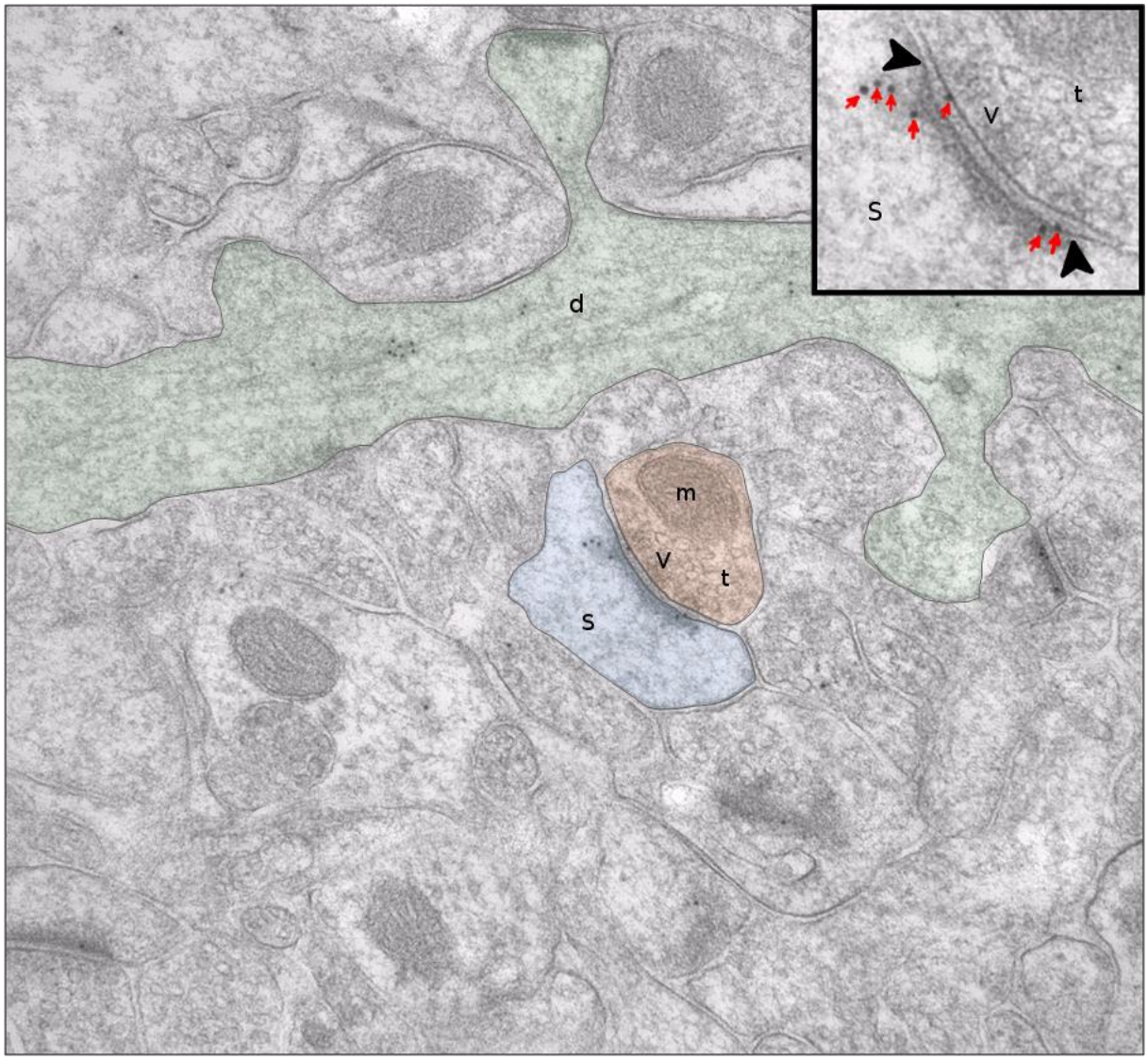

Figure 1.6 A cropped view of stratum radiatum in CA1 by electron microscopy. Green = stem dendrite (d), red = presynaptic terminal (t), blue = dendritic spine (s). The PSD can be seen as a dark «cloud» on the postsynaptic membrane due to all the protein complexes located there, making it electron-dense. The small round circles are vesicles (v) containing neurotransmitters (glutamate). Mitochondria (m) can be seen as dark circles with infoldings of their double membrane. The upper right corner shows a magnified view of the synaptic cleft with 10 nm gold particles (red arrows) coupled to antibodies recognizing ionotropic glutamate receptors in the PSD (length of PSD enclosed

by black arrow heads). Gold particles outside the PSD may be due to unspecific binding of the antibody or anterograde transport of receptors along the dendrites.

1.11 Effects of heart failure on the hippocampus

Hippocampus, and especially the CA1 subfield, has been shown to be particularly vulnerable to ischemia (Schmidt-Kastner and Freund, 1991; Zhu et al., 2012). It is therefore a suitable area to study changes in the brain that might arise due to HF, and also because it is known to be an important brain area for many the cognitive deficits resulting from HF. Not many studies have examined synaptic changes specifically related to HF or other cardiovascular diseases. However, in one study, data obtained by electron microscopy showed increased length and thickness of PSDs in stratum radiatum of CA1 shortly after ischemia (Kovalenko et al., 2006). Another study showed a switch in the expression of AMPA receptor subunits in CA1 following global ischemia, where the expression of the GluA2 subunit was reduced (Pellegrini-Giampietro, 1992). As previously mentioned, the GluA2 subunit is responsible for the Ca^{2+} impermeability of AMPA receptors. The reduction of GluA2 expression was linked to an increased influx of Ca^{2+} and a subsequent activation of the apoptotic pathway in neurons. This provides a possible explanation to why neurons in CA1 typically die first during ischemia compared to neurons in the other subfields of the hippocampus. The increased influx of Ca^{2+} and the presence of apoptotic markers, such as cytochrome c located in the cytosol, have been shown by others as well (Sugawara et al., 1999).

1.12 Mitochondria and uracil-DNA glycosylase 1

Mitochondria are energy supplying organelles found in most eukaryotic cells. The energy is supplied in the form of adenosine triphosphate (ATP), which is synthesized during oxidative phosphorylation. Although most of the mitochondrial genome has been relocated to the nucleus during evolution, some of the genes have been kept inside the mitochondrion, the so called mtDNA (Friedmann and Nunnari, 2014). The protein-encoding part of the mtDNA codes for proteins involved in the electron transport chain and ATP synthesis (Falkenberg et al., 2007). Proteins involved in replication, transcription and DNA repair of the mtDNA are

encoded in the nucleus. One of the DNA repair enzymes is uracil-DNA glycosylase (UNG).

UNG is a DNA repair enzyme which recognizes uracil in DNA through its uracil-binding pocket located near one end of the DNA-binding groove. Its biological function is to prevent mutagenesis by cleaving the N-glycosylic bond of uracil and initiate the base excision repair (BER) pathway (Lindahl and Wood, 1999). Two versions of the UNG protein exist in the cell: UNG1, which is transported to mitochondria, and UNG2, which is transported to the nucleus (Slupphaug et al., 1993). The two UNG proteins are encoded by the same gene that has different promoters and undergoes alternative splicing (Nilsen et al, 1997). The C-terminal 269 amino acids are identical, while their N-terminals are unique and function as a sorting signal for which organelle it translocates to. The human UNG1 version is translocated to mitochondria only, whereas the murine version is not as specific and translocates to mitochondria and the nucleus (Nilsen et al., 2000; Otterlei et al., 1998). UNG1 and UNG2 are expressed in different amounts depending on cell type. Neurons and cardiomyocytes, for example, contain a high proportion of mitochondria due to high energy demand and therefore express high levels of UNG1.

1.13 mutUNG1 expressing heart failure mouse model

The tremendous working capacity of the heart demands a very high energy supply in the form of ATP. In fact, approximately 30% of a cardiomyocyte's total volume is comprised of mitochondria (Barth et al., 1992). An inducible transgenic mouse model expressing a mutated version of human uracil-DNA glycosylase 1, mutUNG1, has previously been generated for studying heart cells with defect mitochondria (Lauritzen et al., 2014). In this model, a single amino acid has been substituted in the UNG1-enzyme's catalytic site, resulting in an enzyme that removes not only uracil, but also thymine, from DNA. The outcome is continuous induction of high levels of apurinic/apyrimidinic (AP) sites throughout the mtDNA leading to mtDNA damage and mitochondrial dysfunction. Mice with this phenotype typically live for roughly two months after induction, before dying from congestive heart failure.

By utilizing molecular biology tools like the Tet-on system, expression of mutUNG1 can be regulated both spatially and temporarily. Two genetic elements are involved: a reverse tetracycline transactivator (rtTA) and a responding Tet-promoter. The rtTA binds to the Tet-promoter in the presence of doxycycline, a tetracycline analogue, which initiates transcription of mutUNG1 (figure 1.7). Therefore, by either adding or removing doxycycline from the mouse's diet, one can turn on or off transcription, respectively. Expression of mutUNG1 will be limited to cardiomyocytes by having the transactivator gene under regulation of the myosin heavy chain α (MHCα) promoter.

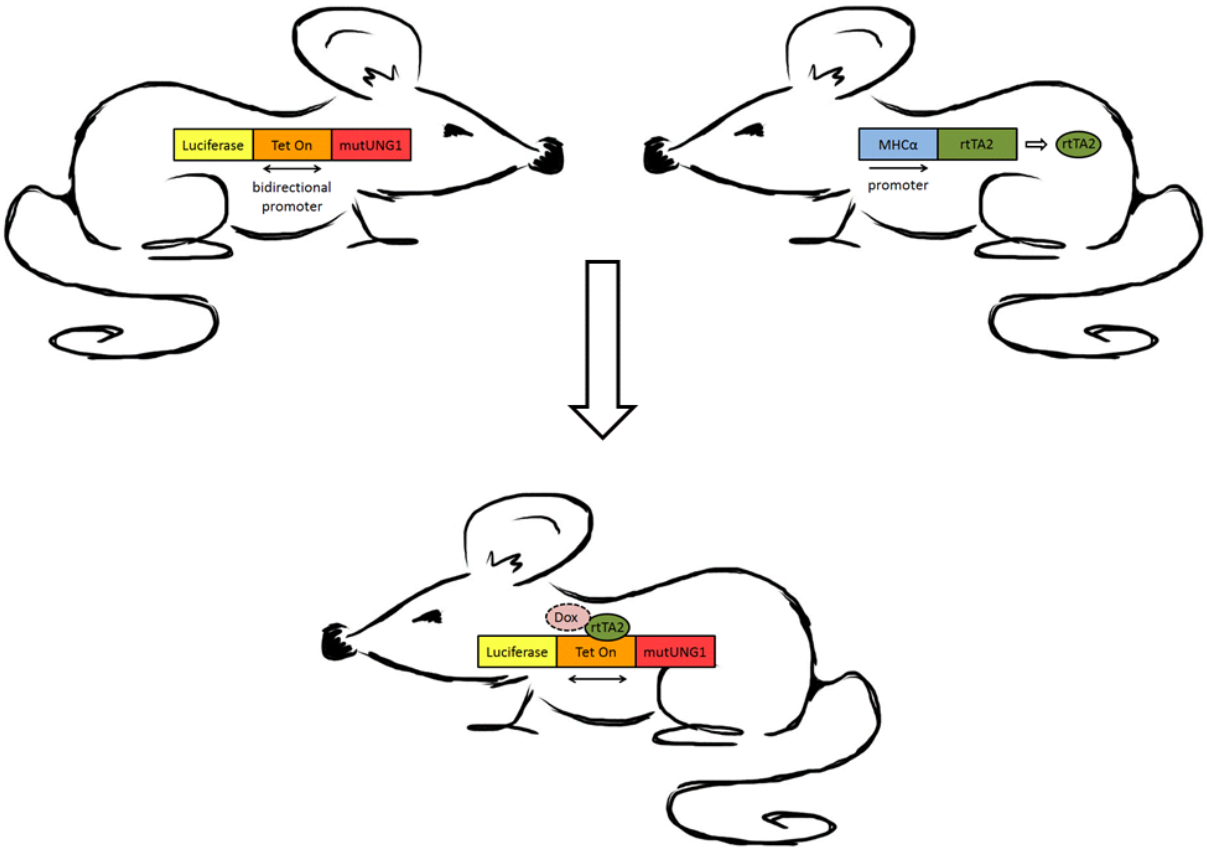

Figure 1.7 The mutUNG1 expressing heart failure model. Expression of mutUNG1 is under regulation of the Tet-on promoter. The transactivator, rtTA2, is required for gene transcription, but is only able to bind to the Tet-on promoter in the presence of doxycycline (Dox). Dox is given through the diet, and it is therefore easy to switch on and off the gene expression of mutUNG1.

1.14 Questions addressed

A decline in cognitive abilities is linked to heart failure. Hippocampus is known to be involved in many of the cognitive functions affected, like memory, learning and spatial navigation. LTP and LTD are thought to be the cellular mechanisms of these functions, and alterations in expression of ionotropic glutamate receptors might provide a possible explanation to some of the cognitive deficits of heart failure patients. The CA1 subfield of the hippocampus has been widely studied when it comes to LTP and LTD, and it is also a brain area that is extra vulnerable to alterations in blood flow. In this thesis, a mutUNG1 heart failure mouse was therefore used as a model organism to address the following questions when comparing it to healthy wild type mice:

1. Are there differences in gene expression of AMPA and NMDA receptor subunits in the hippocampus? This was addressed by quantitative polymerase chain reaction (qPCR).

2. Are there differences in the number of AMPA and NMDA receptors and/or subunit composition at the protein level in Schaffer collateral-CA1 synapses showing immunogold labelling? This was addressed by quantitative postembedding immunogold electron microscopy.

3. Are there morphological changes, in the form of PSD length, in the same Schaffer collateral-CA1 synapses showing immunogold labelling? This was addressed by postembedding immunogold electron microscopy.

2 Materials and methods

2.1 Experimental animals

- All experimental animals were four months of age at the time of death.
- Hippocampus from three FVB/N wild type mice (ID 6, 33 and 39) and three transgenic mutUNG1 expressing FVB/N mice (ID 4, 42 and 98) were used to analyze gene expression by qPCR.
- One half (sagittal cut) of a FVB/N wild type mouse was used to obtain protein homogenate to analyze antibody specificity by Western blot.
- Hippocampi from six FVB/N wild type (ID 6233-03, 6234-02, 6235-02, 6236-02, 6237-02 and 6238-02) and six transgenic mutUNG1 expressing FVB/N mice (ID 6239-03, 6240-02, 6241-02, 6242-02, 6243-02 and 6244-02) were used to analyze protein expression and PSD length by postembedding immunogold electron microscopy.

2.2 Reagents, solutions, kits and antibodies

See appendix for all reagents, solutions, kits and antibodies that were used.

2.3 Quantitative polymerase reaction (qPCR)

qPCR was performed to check for differences in gene expression of AMPA and NMDA receptor subunits in the hippocampus of wild type and mutUNG1 expressing mice. The whole procedure is described below and comprises RNA isolation and quantification, complementary DNA (cDNA) synthesis and cDNA amplification.

2.3.1 RNA isolation from hippocampus

Because brain tissue contains high amounts of lipid, the RNA isolation was performed using the RNeasy Lipid Tissue Mini Kit (QIAGEN, Netherlands), a kit designed for extracting RNA from fatty tissue. Hippocampal tissue (30 mg) from each mouse was transferred to separate Lysing Matrix D tubes, containing small ceramic beads, in combination with QIAzol Lysis Reagent. The tubes were inserted into a FastPrep-24™ Instrument (MP Biomedicals) and shaken for 40 seconds at a speed setting of 6 m/s. Chloroform was added for the separation of the homogenate into three phases after centrifugation: an upper, aqueous phase containing RNA, an interphase containing DNA, and a lower, organic phase containing proteins. The upper phase was transferred to a new eppendorf tube with the addition of 70% ethanol and subsequently transferred to a spin column placed in a collection tube. RNA will stick to the spin column's membrane after centrifugation. An additional step with DNase treatment was performed to get rid of any DNA that might have been transferred along. The membrane was then washed with ethanol-containing buffer, and the spin column was subsequently transferred to a new collection tube where RNA was eluted by adding RNase free water followed by centrifugation.

2.3.2 Quantification and evaluation of RNA

The amount of isolated RNA was measured by the use of a NanoDrop 2000c instrument (Thermo Scientific, USA), which measures the absorbance during exposure of the RNA solution to ultraviolet light at 260 nm. 1 µl of RNA was pipetted onto the pedestal before registering the quantification number. This was done twice for each sample, giving an average, and a third time if the two first measurements differed significantly.

RNA quality was checked on a 1.5% agarose gel, containing ethidium bromide (EtBr). When bound to the RNA, EtBr emits fluorescence when exposed to UV-light. RNA, diluted in RNase-free water, together with loading buffer, were pipetted into six individual wells; one for each mouse sample. The gel was run for 40 minutes in 1X TAE buffer at 100 Volts for separating the RNA based on size. Fluorescence was detected during exposure by UV-light in a Gel Doc™ EZ imager (Applied Biosystems, USA).

2.3.3 Complementary DNA (cDNA) synthesis

cDNA was synthesized from total RNA using the High Capacity RNA-to-cDNA kit (Applied Biosystems, USA). 20 µl reaction mixtures containing 2 µg of RNA template, RT-buffer and RT Enzyme mix were set up according to manufacturer's protocol. In this reaction mixture, a mix of oligo(dT) primers and random primers were used. Oligo(dT) primers anneals specifically to the poly(A) tail of mRNA, and random primers are more efficient if the RNA contains secondary structures. The combination of both increase data quality. Reverse transcription PCR (RT-PCR) was performed on a GeneAmp® PCR System 9700 (Applied Biosystems, USA). The thermal cycling conditions were set to 37 °C for 60 min and 95 °C for 5 min, required for transcription and denaturation respectively.

2.3.4 Amplification of cDNA

Quantitative amplification of cDNA was done by qPCR in combination SYBR green, allowing amplification to be observed in real time. SYBR green is not as specific as sequence-specific fluorescent probes, as it will bind to all double-stranded DNA, whether it be the gene-of-interest (GOI), pseudo genes or primer dimers. Specific primers is therefore of great importance in order to avoid false signs. Several primer pairs for each gene were obtained from *http://mouseprimerdepot.nci.nih.gov/* and literature, and melting curve analysis was performed to determine the best suited primer pairs (table 2.1). The primer sequences were confirmed to be included in all splice variants of the genes by performing BLAST searches.

Gene	Sequence (5'-3')	Length	Tm	GC %
Gria1	F: CCTTTGGAGAACTGGGAACA	20	64.0	50.0
	R: GCTTTGTCACAACTCACGGA	20	64.0	50.0
Gria2	F: CCTCTTGAAAACTGGGAGCA	20	64.2	45.0
	R: ATTTCGGGTAGGGATGGTTC	20	63.7	50.0
Gria3	F: TCCAAAGATAGCATACACCC	21	62.6	47.6
	R: CACCAACCAGAACACCACTG	20	64.3	55.0
Gria4	F: GAGCACTGCAGAAGGAGGTC	20	64.2	60.0
	R: CTGCCAACAGTTTTGCTGTG	20	64.5	50.0
Grin1	F: TGGGCTTGACATACACGAAG	20	63.7	50.0
	R: GCCAGGAGGAGAGACAGAGA	20	63.8	60.0

Grin2a	F: TGGAAGCTCCAAACTGGAAG	20	64.2	50.0
	R: GTGGCTCAGATGCTGGATTT	20	64.2	50.0
Grin2b	F: AGGTGGTGACGATGGAGAAG	20	64.2	55.0
	R: ATCCATGGGGGCTCATCTA	19	64.2	52.6
Grin2d	F: CCTGCCTTGAGCTGAGTGAG	20	65.3	60.0
	R: CCACGGAGAAGAATATCCGA	20	63.9	50.0
Grin3a	F: GACATGGGGAGCATCCGGCAG	21	75.1	66.6
	R: CTTCTGTCCTCAGCTCCTCCAC	22	66.5	59.0
Gapdh	F: TCGTCCCGTAGACAAAATGGT	21	52.4	47.6
	R: CGCCCAATACGGCCAAA	17	58.8	49.5

Table 2.1 Primer pairs for qPCR. The mouse versions of the gene names are given. Gria = AMPA receptor subunit, Grin = NMDA receptor subunit.

Expression levels of the following genes were analyzed: GluA1, GluA2, GluA3, NR1, NR2A, NR2B, NR2D and NR3A. The reaction plate setup included cDNA triplicates from each sample, standard curves for the GOI and reference gene (GAPDH) and no template controls. 5 ng of cDNA was used as template, and a tenth fold dilution of 0.01 – 0.1 – 1 – 10 – 100 ng for the standard curves. Standard curves were created by pooling cDNA from all the samples, assuming that all the RT reactions were performed with the same efficiency. The volume in each well consisted of 10 µl SYBR green master mix, 0.2 µl forward primer, 0.2 µl reverse primer, 7.6 µl MQ water and 2 µl cDNA template, giving a total of 20 µl. The qPCR was performed on a StepOnePlus^{TM} Real-Time PCR System (Applied Biosystems) with a two-step cycling program of 40 cycles: denaturation at 95 °C for 15 sec and annealing/elongation at 60 °C for 1 min. Each program was ended with a melting curve analysis to ensure amplification of only one product (figure 2.1a).

2.3.5 Normalization of data

The standard curve method was used for analyzing the data. The number of amplification cycles required for SYBR green fluorescence to be detected over a defined threshold, the C_T value, was presented in an amplification plot (figure 2.1b). Standard curves were generated for the GOI and an endogenous reference gene, Glyceraldehyde 3-phosphate dehydrogenase (GAPDH) (figure 2.1c). GAPDH was chosen as the reference gene, as it is a housekeeping gene and should be present at a consistent level across all samples, ensuring credibility of the data. If the expression of the reference gene differs across the samples, it might indicate pipetting errors or variability in the RT reaction efficiency. The C_T values, in combination

with the standard curve, were used to calculate gene copy numbers (figure 2.1d). The GOI's copy number was then divided by the copy number of GAPDH, normalizing the value. Calculations were performed in Microsoft Excel 2010 (Microsoft Corporation, USA).

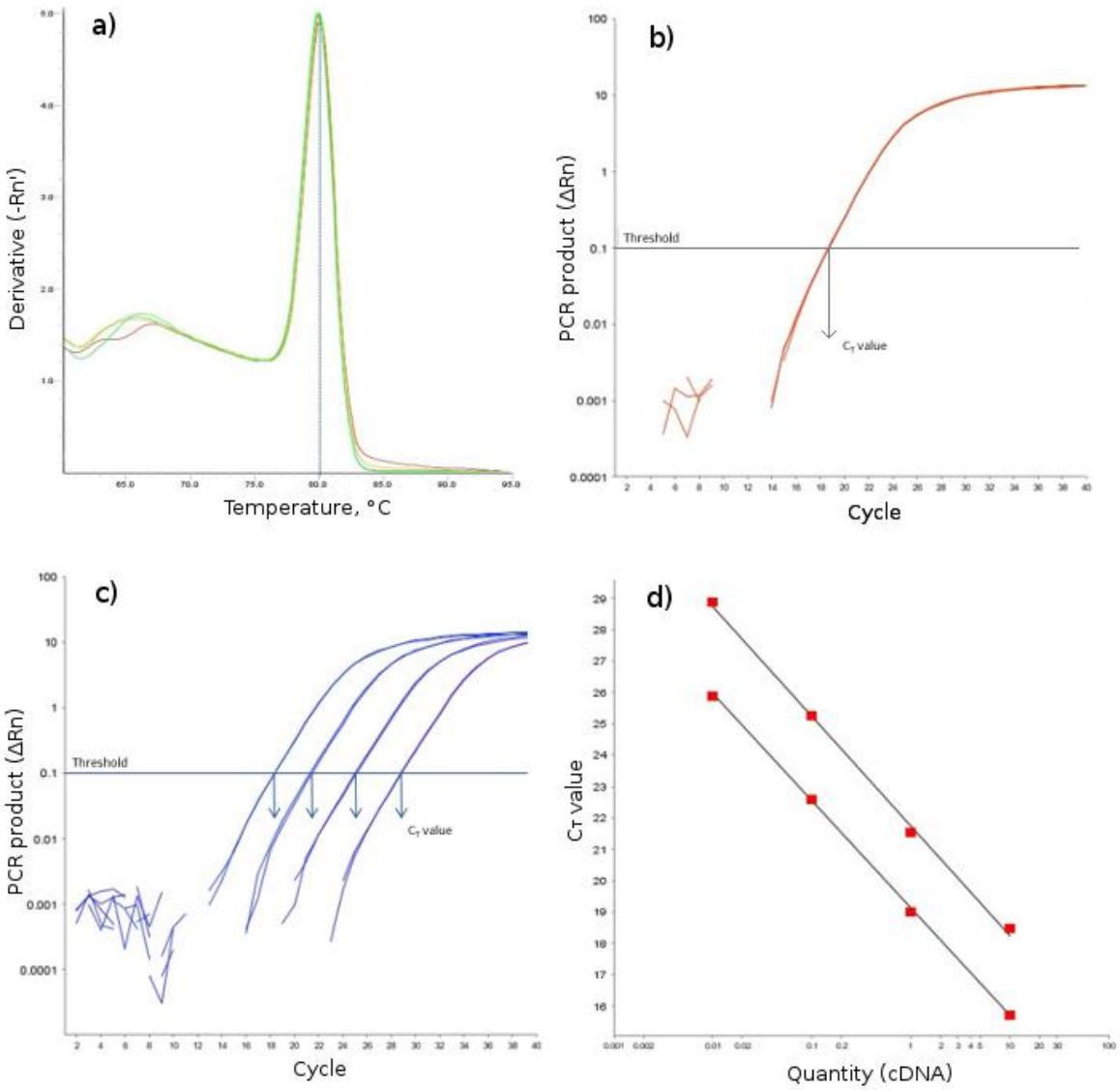

Figure 2.1 Graphical presentation of qPCR. a) Melting curve for the assessment of amplified product. Observation of a single peak indicates primer specificity in that only one product has been amplified. b) An amplification plot showing the number of amplification cycles needed to reach a defined threshold. This number of cycles is termed the C_T value. c) An example of an amplification plot for the standard curve (four ten-fold dilutions being shown). d) Quantification of cDNA by the use of a standard curve. One standard curve for the GOI and one for the normalizing gene (GAPDH) is shown. The copy number obtained for the GOI is divided by the copy number obtained for GAPDH, normalizing the value.

2.3.6 Statistical analysis

The two-tailed Mann-Whitney *U* test was used to analyze the data. It is as a more robust test than the student's *t*-test because of the sample size, which is too small to assume it is normally distributed. Difference in gene expression is presumed if $P < 0.05$. The analysis was performed in GraphPad Prism 6 (GraphPad Software, inc., USA).

2.4 Western blotting

Western blotting was performed to check the specificity of the antibodies to be used for immungold labelling: anti-GluA1, anti-GluA2&3, anti-NR1, anti-NR2A&B. The whole protocol is described below.

2.4.1 Protein isolation

One half of a brain (sagittal cut) from wildtype mouse was transferred to a Lysing Matrix D tube. 1 ml RIPA buffer, containing protease inhibitor, was added. The RIPA buffer can be used for extraction of both soluble and membrane proteins. The tube was inserted into a FastPrep®-24 Instrument (MP Biomedicals, USA) and shaken at 6 m/s for 40 sec, before being put on ice for 2 hours, followed by centrifugation at 12100 x g for 8 min. The supernatant was then pipetted into a new eppendorf tube, excluding the fatty tissue at the bottom. A total of ~800 µl was obtained and aliquoted into 50 µl samples (stored at -80 °C).

2.4.2 Protein quantification

The amount of protein isolated was determined by using the BCA Protein Assay Kit (Pierce, Thermo Fisher Scientific, USA). This assay utilizes the biuret reaction, where cupric ions (Cu^{2+}) are reduced to cuprous ions (Cu^{+}) in the presence of protein, followed by a second reaction in which the resulting cuprous ions react and form complexes with bicinchoninic acid (BCA). The BCA-Cu^{+} complexes yield a purple colour, showing the strongest absorbance at 562 nm that is linear with increasing protein concentrations.

Stock solution	BSA, 2mg/ml	1% SDS Buffer	Concentration
Std 1	60 µl stock	-	2000 µg/ml
Std 2	60 µl stock	60 µl	1000 µg/ml
Std 3	84 µl stock	140 µl	750 µg/ml
Std 4	20 µl stock	60 µl	500 µg/ml
Std 5	20 µl stock	140 µl	250 µg/ml
Std 6	40 µl Std 5	60 µl	100 µg/ml
Std 7	20 µl Std 5	80 µl	20 µg/ml
Std 8	-	60 µl	0 µg/ml

Table 2.2 Standard curve setup for protein quantification.

A flat bottom 96-well microplate (Thermo Scientific, USA) was used for setting up the BCA assay. A standard curve was prepared by diluting bovine serum albumine (BSA) with 1% Sodium dodecyl sulfate (SDS) buffer (table 2.2). The isolated protein homogenate was diluted 1:5, 1:10 and 1:20. Standards, undiluted and diluted protein samples were pipetted in 10 µl triplicates. The BCA assay reagents were mixed 50:1 (24.5 ml of reagent A with 500 µl of reagent B), and 200 µl of this reagent mixture was added to each well. The microplate was covered with a thin plastic film and mixed for 15 min on a rotary shaking table, before being incubated at 37 °C for 30 min. Absorption was then measured at 562 nm by the use of a Spectrophotometer (SPECTROstar, Omega, BMG Labtech, Germany). The standard curve was used to calculate the protein concentration in the unknown samples (Appendix F).

2.4.3 Separation of proteins by SDS-PAGE

Sodium dodecyl sulfate polyacrylamide gel electrophoresis (SDS-PAGE) was used for the separation of proteins based on the size alone. SDS is an anionic detergent that linearizes proteins and imparts a negative charge. The longer the linear protein is, the more negative charge it has. The original conformation and charge of the protein, which would otherwise have affected the mobility, are therefore excluded.

The protein homogenate were diluted to approximately 2 µg/µl with sample buffer, before being mixed properly and incubated at 60 °C for 5 min (appendix F). Preparation of 1X

Running buffer was carried out by adding 450 ml of distilled water to 50 ml of 10X Running buffer. A 4-20% Criterion^{TM} Precast Gel was prepared by removing the white tape at the bottom of the gel cassette, for later allowing the electric current to go through, and placed into a Criterion^{TM} Cell tank (Bio-Rad Laboratories, USA). Approximately 50 ml of the running buffer was added to the upper buffer chamber, covering the wells, before gently removing the comb from the top of the gel. The wells were washed by pipetting running buffer into them. 5 ul of the protein standard ladder and different volumes of the prepared samples (10, 20 and 40 ul) were pipetted by the use of a micropipette with gel-loading tips. The remaining loading buffer, approximately 400 ml, was poured into the lower buffer chamber. The casset's lid was put on top, and the leads were plugged into the power source. The electrophoresis was run for 1 hour on 200 V.

2.4.4 Electrophoretic transfer of proteins

Electrophoretic transfer of proteins is the process of transferring, or "blotting", proteins from the separating acrylamide gel onto a solid support matrix by the use of an electric field. Due to the treatment with SDS, the negatively charged proteins will migrate towards the anode. The support matrix used here is a nitrocellulose membrane, which has high protein-binding affinity and can be used with a variety of detection methods. The transfer can either be "semi-dry" or "wet". The latter was carried out, in which the blotting takes place in a tank filled with blotting buffer. Wet transfer yields a higher transfer efficiency of bigger proteins.

The gel cassette was opened with a gel knife, and the upper and lower parts of the gel were cut away. A "blotting sandwich" was prepared by stacking filter pads, filter paper and the gel, together with a nitrocellulose membrane, in the middle (figure 2.2), before being placed in a plastic cassette. All parts were soaked in blotting buffer before assembly, and a small roller tool was used to remove air bubbles between the gel and the nitrocellulose membrane. Since the current generates a lot of heat, a cooling element was placed in the back, and a magnet was put in the tank, which was placed on a magnetic stirrer. The Criterion^{TM} Blotter tank (Bio-Rad Laboratories, USA) was filled with blotting buffer and the lid was put on. 50 V was applied for 2 hours.

After the run, the sandwich was opened, and the nitrocellulose membrane was taken out by

carefully removing the fiber pads. The membrane was left to air dry on a piece of paper.

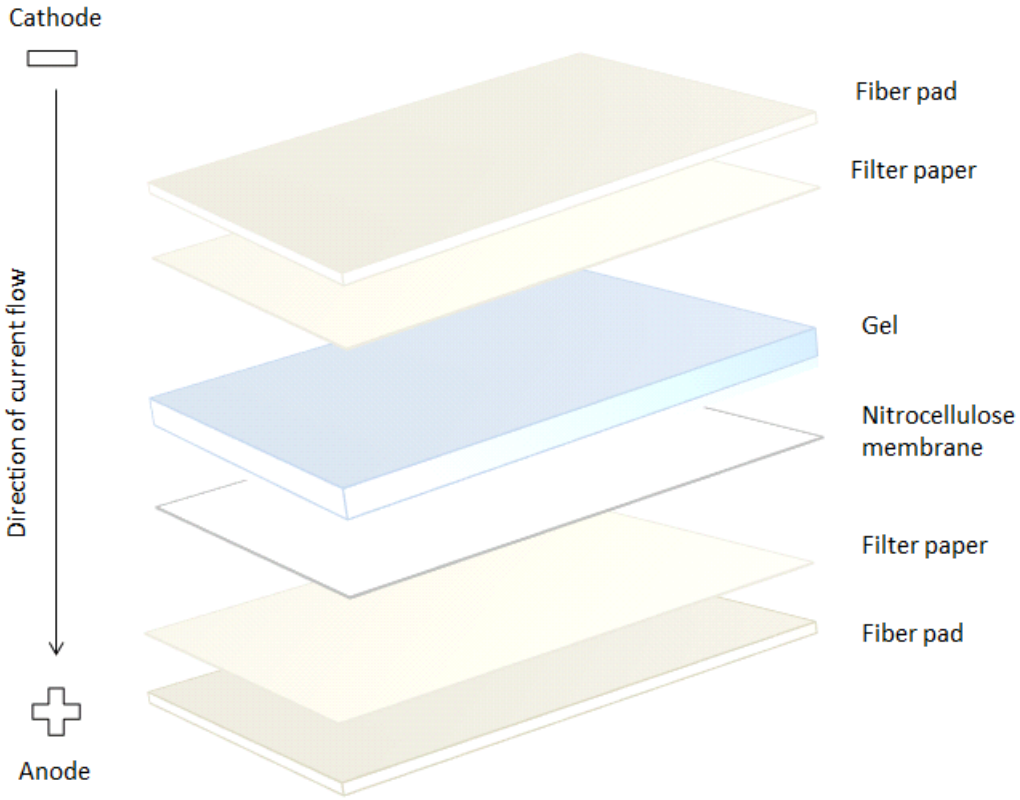

Figure 2.2 Illustration of a "blotting sandwich". The proteins, having a negative charge due to treatment with SDS, will travel towards the anode when applying an electrical field.

2.4.5 Incubation with antibodies

The nitrocellulose membranes were incubated in blocking solution containing Tris-buffered saline Tween (TBST) w/ 4% bovine serum albumin (BSA)) for 1 hour on an electric shaker, before being rinsed in TBST for 3x10 min. This step blocks the protein-free areas of the membrane, preventing antibodies from binding to the membrane and thereby reducing the background labelling. Primary and secondary antibodies were diluted in different concentrations of less concentrated blocking solution (TBST w/1% BSA):

Primary antibodies:	
Rabbit Anti-GluA1 IgG	1:200
Rabbit Anti-GluA2&3 IgG	1:1000
Mouse Anti-NR1 IgG	1:300, 1:900, 1:2700
Rabbit Anti-NR2A&B IgG	1:1000

Secondary antibodies:	
Donkey anti-rabbit IgG, HRP-linked	1:20 000
Rabbit anti-mouse IgG, HRP-linked	1:20 000

The nitrocellulose membranes were incubated overnight in primary antibody solution at room temperature (negative controls in blocking solution without primary antibody) on a fixed angle platform rocker, before being rinsed in TBST for 3x10 minutes. The membranes, including negative controls, were thereafter incubated in secondary antibody solution for 1 hour at room temperature on an electric shaker, before being rinsed in TBST for 3x10 minutes.

2.4.6 Detection and visualization of proteins

The detection of protein bands was achieved by chemiluminescence. SuperSignal® West Dura Extended Duration Substrate kit (Pierce, Thermo Fisher Scientific, USA) was used to detect the blotted proteins. The nitrocellulose membranes were incubated for 5 min in enhanced chemiluminescence (ECL) substrate (2 ml of Stable Peroxidase Buffer mixed with 2 ml of Luminol/Enhancer Solution). Horseradish peroxidase, which is linked to the secondary antibody, will in contact with its substrate catalyze a reaction that yields a chemiluminescent product which emits light. The emitted light was detected using a digital imaging system (Image Reader LAS-3000, Fujifilm, Japan).

2.5 Immunogold electron microscopy

Postembedding immunogold labelling, in combination with transmission electron microscopy, was used to quantitate the average number of ionotropic glutamate receptor subunits in Schaffer collateral-CA1 synapses of the hippocampus and to measure the PSD length of those synapses that did show labelling.

The tissue fixation and dissection, lowicryl embedding and sectioning were performed by laboratory workers at the Electron Microscopic Laboratory, Department of Anatomy, University of Oslo (Norway). The ultrathin sections were received ready for immunogold labelling. The protocols are nevertheless included here to explain the whole method.

2.5.1 Tissue fixation and dissection

The mice were anesthetized according to animal welfare laws followed by transcardial perfusion with fixative containing 0.1% glutaraldehyde and 4% formaldehyde in phosphate buffer (PB). After tissue fixation, the hippocampi were dissected out into 1 mm^3 specimens, followed by cryoprotection in increasing concentration of glycerol: 10%, 20% and 30% in PB for 30 minutes at room temperature each time and finally at 4 °C over night.

2.5.2 Lowicryl embedding

The specimens were embedded in Lowicryl HM20, which is a water insoluble, acrylic resin, allowing the specimens to be sectioned into ultrathin sections. The specimens were first quickly frozen in liquid propane. This rapid cooling avoids the formation of ice crystals within the tissue. The specimens were then dehydrated and treated with 1,5% uranyl acetate in anhydrous methanol at -90 °C for 30 hours, followed by a stepwise temperature increase of 4 °C from -90 °C to -45 °C. Dehydration was followed by infiltration of Lowicryl HM20, a water-insoluble acryl-based resin, and left overnight before being exposed to UV-light at -45 °C for 24 hours. The UV-light leads to polymerization of the resin, making it hard. This was followed by a stepwise temperature increase of 1 °C until 0 °C was reached. Exposure to UV-light was then continued for 35 hours. After polymerization, the resin blocks were stored

at room temperature.

2.5.3 Ultrathin sectioning

The resin blocks were trimmed to get rid of excessive resin. The trimmed resin blocks were then cut with a diamond knife into ultrathin sections of approximately 90 nm on a microtome (Reichert Ultracut S-2.GA-E-12/92, Leica Microsystems, Germany). This thickness is required when looking at the tissue in an electron microscope. A larger thickness will prevent the electron-beam from passing through the tissue, thus making it impossible to visualize the tissue morphology. The ultrathin sections were transferred onto nickel mesh grids and left at room temperature.

2.5.4 Postembedding immunogold labelling

Before starting with immunogold labelling, the primary and secondary antibody solutions were prepared by diluting the primary antibodies in Tris-buffered saline Triton (TBST) w/ 2% human serum albumin (HSA) and secondary antibodies in TBST w/ 2% HSA and polyethylene glycol (PEG) added.

Primary antibodies:	
Rabbit Anti-GluA IgG	1:100
Rabbit Anti-GluA2&3 IgG	1:50
Mouse Anti-NR1 IgG	1:300
Rabbit Anti-NR2A&B IgG	1:100

Secondary antibodies:	
Goat anti-rabbit IgG	1:20
Goat anti-mouse IgG	1:20

An incubation chamber was made by covering the bottom of a large petri dish with Parafilm on top of moistened filter paper, thus preventing the droplets to be applied from drying out during incubation. The protocol was performed according to Bergersen et al., 2008, as

followed:

Etch the resin with 2% H_2O_2 for 10-15 min. This will increase the availability of antigen sites, thereby increasing the sensitivity.

Rinse in PB for three times 15 sec. (new beaker after four grids)

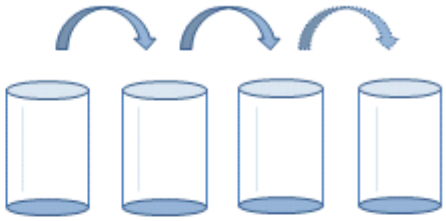

Incubate for 10 min in glycine/borohydride to neutralize free aldehyde groups. This will reduce nonspecific background labeling.

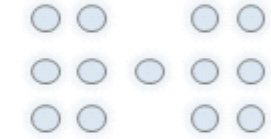

Rinse in TBST for three times 15 sec .

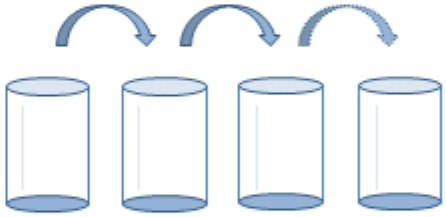

Incubate for 10 min in blocking solution, containg soluble proteins . The soluble proteins will reduce nonspecific background labeling by competing with proteins in the tissue for binding to antibodies.

Transfer sections to primary antibodies in blocking solution. Incubate in petridish over night at room temperature.

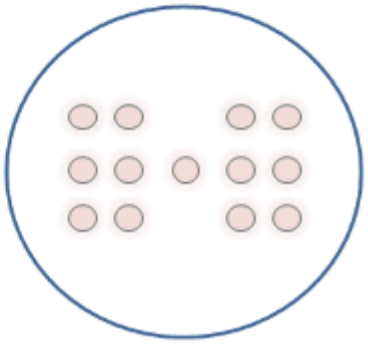

Rinse in TBST for three times 15 sec. (negative control in separate beakers)

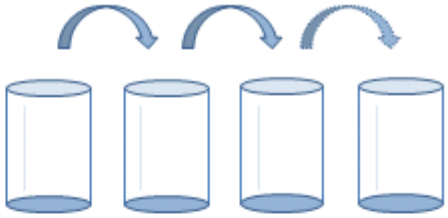

Rinse in droplets of TBST for 10 min. Repeat previous step and then repeat this step.

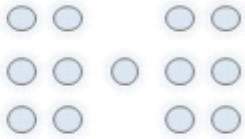

Incubate in blocking solution w/PEG for 10 min.

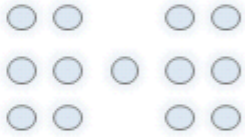

Transfer sections to seconday antibodies diluted 1:20 in blocking solution w/PEG. Incubate for 2 hours at room temperature.

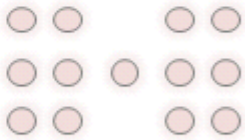

Rinse in MQ water for three times 10 sec, before letting the sections dry.

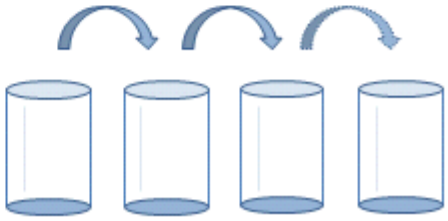

2.5.5 Contrasting of ultrathin sections

The sections were counterstained with 1% uranyl acetate and 0.3% lead citrate to make cellular compartments easier to differentiate. The uranyl acetate and lead citrate were pipetted into two separate eppendorf tubes and centrifuged for 5 minutes at 2000 rpm to make sure that any precipitates stayed at the bottom. The uranyl acetate was kept in the dark to avoid precipitation by covering the eppendorf tube with silver foil. The sections were incubated in 30 µl droplets of 1% uranyl acetate for 10 minutes, before being rinsed 3x10 seconds in glass beakers with MQ water (exchanged the first beaker after three sections). The sections were then air dried at room temperature for 20 minutes. Managing one grid at a time, the sections were incubated in 30 µl of 0.3% lead citrate for 90 seconds, and then rinsed for 3x10 seconds in MQ water, before being put in the gridbox to air dry overnight.

2.5.6 Electron microscopy

All images were acquired by the use of a transmission electron microscope (CM10, Phillips, Germany) and the software program AnalySIS (AnalySIS Soft Imaging Systems Gmbh., Germany). An outline of the section was marked at a magnification of 360X for making it easier to find the right layers in the tissue. The cell body layer of stratum pyramidale was located at a magnification of 2500X before navigating to stratum radiatum, just beneath the cell bodies, were the large stem dendrites easily can be seen. Here, the magnification was increased to 46000X. Excitatory synapses that showed visible pre- and postsynaptic membranes, a synaptic cleft and a visible PSD with immunogold labelling were recorded. Approximately 50 synapses were recorded from each section. The images were given a scale bar of 500 nm before saving them as 8-bit TIFF files for later analysis.

2.5.7 Image analysis

The images were analyzed in ImageJ (Rasband, W.S., National Institute of Health, USA) by the use of the Synapse plug-in developed by Dr. Max Larsson: *http://www.hu.liu.se/forskning/larsson-max/software?l=en*.

The scale bar was used to obtain a scale of 0.9 pixels/nm. Outlines of the pre- and postsynaptic membranes and the PSD were highlighted, and observed gold particles were marked. The number of marked gold particles within 25 nm of the PSD was counted by the Synapse plug-in, representing the number of receptor subunits associated with the PSD (figure 2.3a and b). The PSD length was also measured. The PSD length and number of gold particles were averaged for each mouse and subsequently used to calculate the average for both the WT and mutUNG1 group.

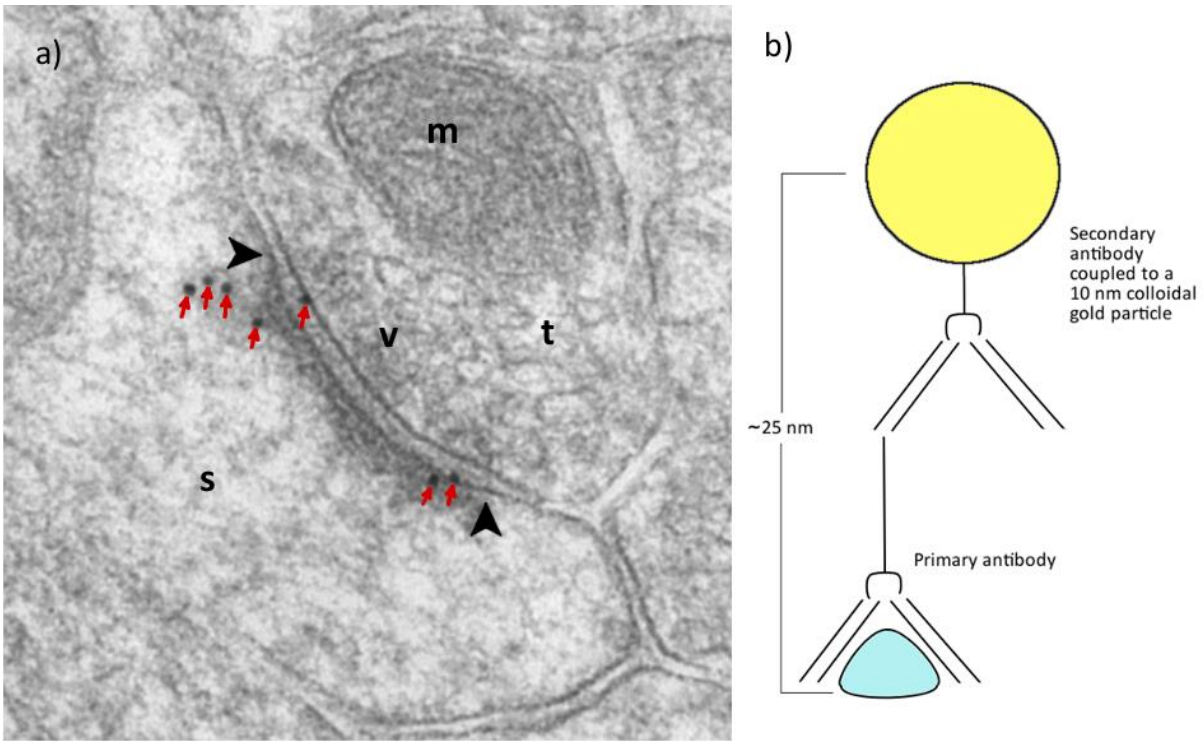

Figure 2.3 a) Electron micrograph of an excitatory synapse in stratum radiatum of CA1. The PSD can be seen as a black cloud because of all the proteins located here, making it electron dense. The black arrows indicate the lateral ends of the PSD, while the red arrows marks the gold particle. Gold particles within 25 nm of the postsynaptic membrane in the PSD were counted. t = presynaptic terminal, v = vesicles, m = mitochondrion, s = postsynaptic spine. b) Illustration of the lateral resolution that is obtained by the immunogold method. The colloidal gold particle is linked to the Fab fragment of the secondary antibody. Antigen is coloured in turquoise.

2.5.8 Statistical analysis

The two-tailed student's *t*-test, where significance is presumed if $P < 0.05$, was used to compare the mutUNG1 group to the WT group. The *F*-test was used to see if equal variances could be assumed or not. The analyses were performed in GraphPad Prism 6 (GraphPad Software, inc., USA).

3 Results

3.1 Gene expression

The RNA used for cDNA conversion by reverse transcription was taken from whole hippocampus. The quality can be seen below in figure 3.1. The rightmost lane is a bit darker than the other lanes and had a marginally weaker band for the 16S rRNA. However, expression levels for GAPDH were the same in all six animals. The RNA in the other lanes seemed intact and did not show any sign of non-degraded genomic DNA.

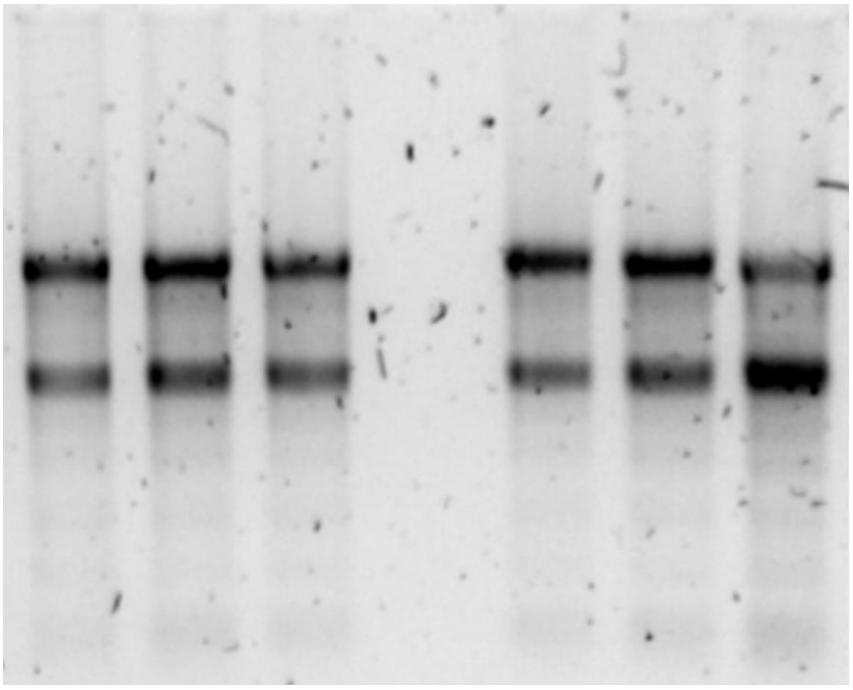

Figure 3.1 RNA separated by gel electrophoresis. Dark bands show 16S and 28S rRNA. The lane furthest to the right (animal ID 49) shows a marginally weaker 16S band and a bit darker lane overall.

qPCR was performed with specific primers for most subunits. Gene expression of AMPA receptor subunits GluA1, GluA2 and GluA3 and NMDA receptor subunits NR1, NR2A, NR2B, NR2D and NR3A were quantified in wild type and mutUNG1 expressing mice for comparison. Expression levels were normalized to GAPDH expression levels, as GAPDH were found to be equally expressed across all samples. The results are presented in figure 3.2.

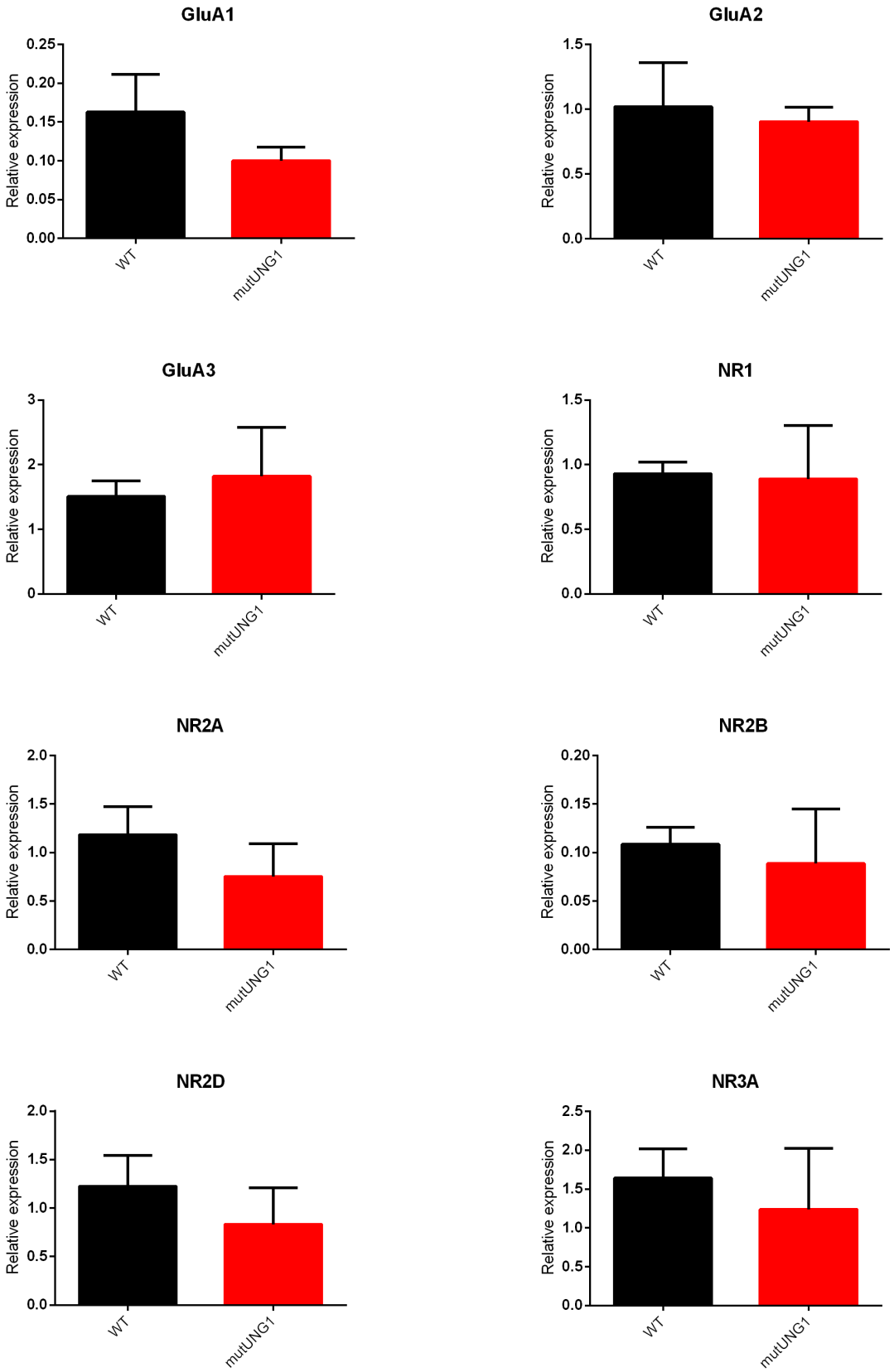

Figure 3.2 Average gene expression levels for AMPA and NMDA receptor subunits in wild type and mutUNG1 expressing mice. The bar charts include standard deviations.

The *P*-values obtained by the Mann-Whitney *U* test were all higher than 0.05, indicating no significant difference (GluA1 = 0.10, GluA2 = 0.70, GluA3 = 0.70, NR1 = 0.70, NR2A = 0.20, NR2B = 0.90, NR2D = 0.40, NR3A = 0.40). The high standard deviations observed are due to large variations within the two groups.

3.2 Western blot

The immunoblots obtained by Western blotting on whole brain homogenate from a wild type mouse show a single, strong band for anti-GluA and GluA2&3 at the expected location, just above 100 kDa. NR1 did show a strong band at the expected location (~120 kDa), but also some weaker bands. However, these additional bands got weaker when reducing the concentration of antibody, while the expected band remained the same (other blots not shown here). NR2A&B showed one strong band at the expected location (~180 kDa), but also one strong band at ~60 kDa.

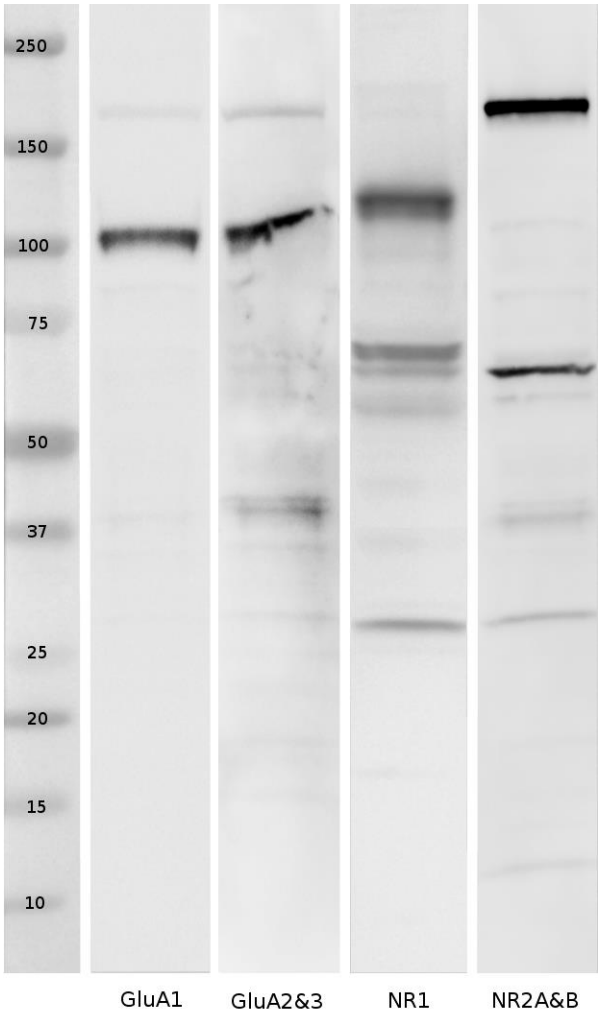

Figure 3.3 Immunoblots for the four antibodies that were tested.

3.3 Immunogold electron microscopy

Even though the qPCR analysis did not show any significant differences in gene expression between the wild type and mutUNG1 expressing mice, this did not mean that any differences at the protein level could be ruled out. Postembedding immunogold labelling in combination with electron microscopy were therefore performed.

Ultrathin sections from the hippocampus of wild type and mutUNG1 expressing mice were labelled with antibodies for GluA1, GluA2&3, NR1 and NR2A&B. Excitatory synapses in the stratum radiatum of CA1 that showed immunogold labelling (figure 3.4) were recorded. The PSD lengths were measured, and the numbers of gold particles were quantified. Recorded synapses that did not contain gold particles within 25 nm of the PSD were excluded when analyzing the data.

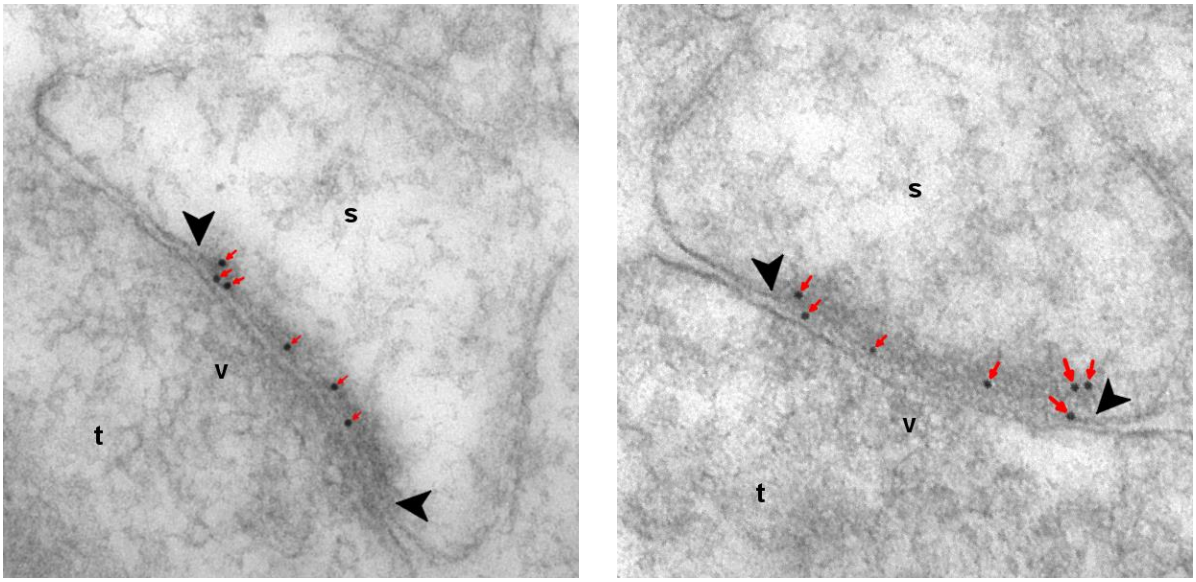

Figure 3.4 Two electron micrographs, one from wild type (left) and one from mutUNG1 (right), of excitatory synapses labelled with GluA2&3 antibodies. The black arrow heads enclose the length of the PSD, while red arrows point to gold particles. t = presynaptic terminal, v = vesicles, s = dendritic spine. The average number of gold particles and the average length of the PSD were compared between the two groups.

Gold particles were counted in PSDs of synapses that did show immunogold labelling (figure 3.5). The *F*-test gave no significant difference for all the data sets, thus assuming equal variances, and the two-tailed student's *t*-test was therefore used. The number of gold particles was very much the same in wild type and mutUNG1 expressing mice, and no statistical significance was observed with *P*-values above 0.05 in all the data sets (table 3.1).

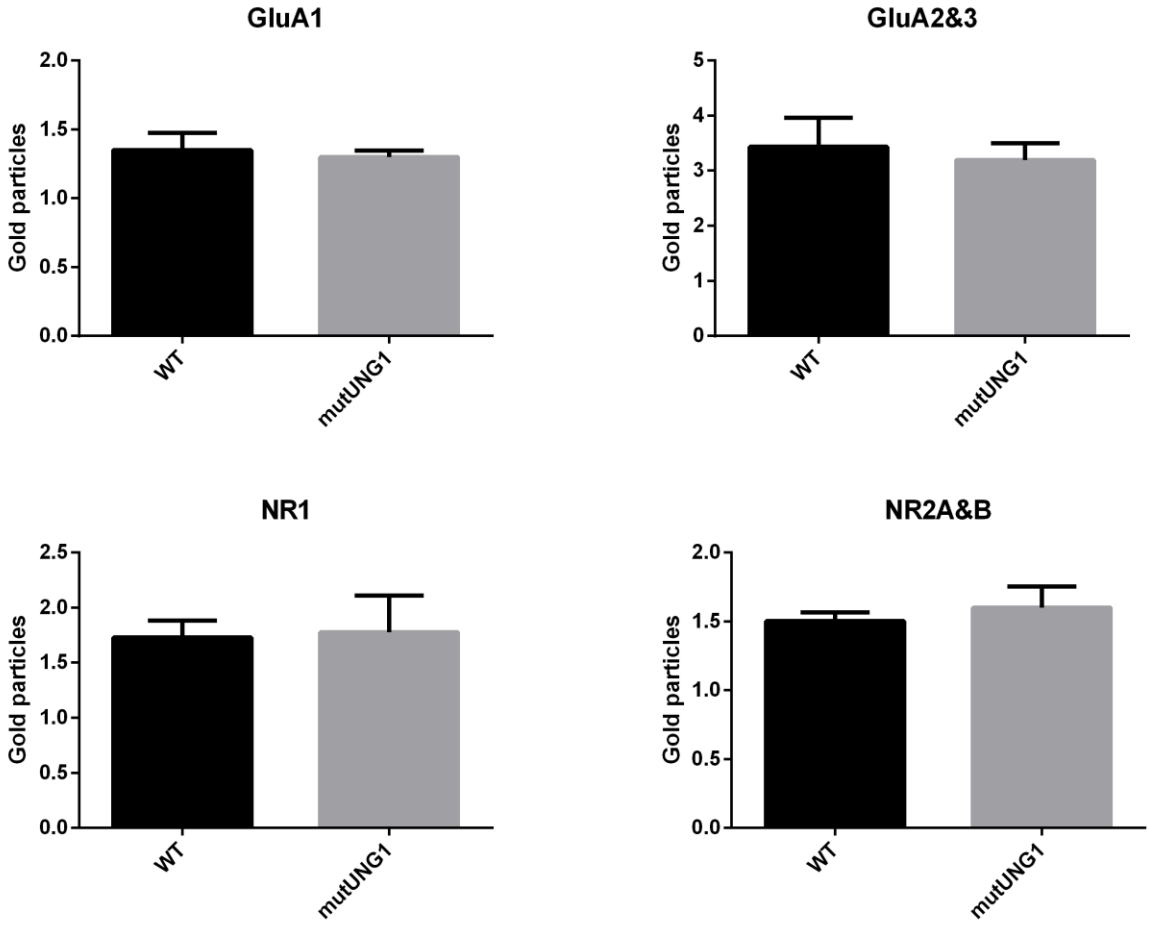

Figure 3.5 A graphical representation of the number of gold particles counted in PSDs of synapses showing immunogold labelling. No significant difference was found between wild type and mutUNG1 expressing mice.

The length of the PSDs in the same synapses containing gold particles were measured (figure 3.6). The *F*-test gave no statistical difference for all except the GluA1 data. The *F*-test for GluA1 gave a *P*-value of 0.0408, meaning that the variance between the two groups is

significantly different. The Welch's two-tailed *t*-test, which does not assume equal variances, was therefore used to compare the PSD lengths of the two groups for GluA. The average PSD length of synapses labelled with anti-GluA2&3 did show a minor difference with 272 nm and 293 nm in wild type and mutUNG1 expressing mice respectively. The other PSD lengths were very similar. The two-tailed student's *t*-test showed no statistical differences, with *P*-values above 0.05 in all the data sets (table 3.2).

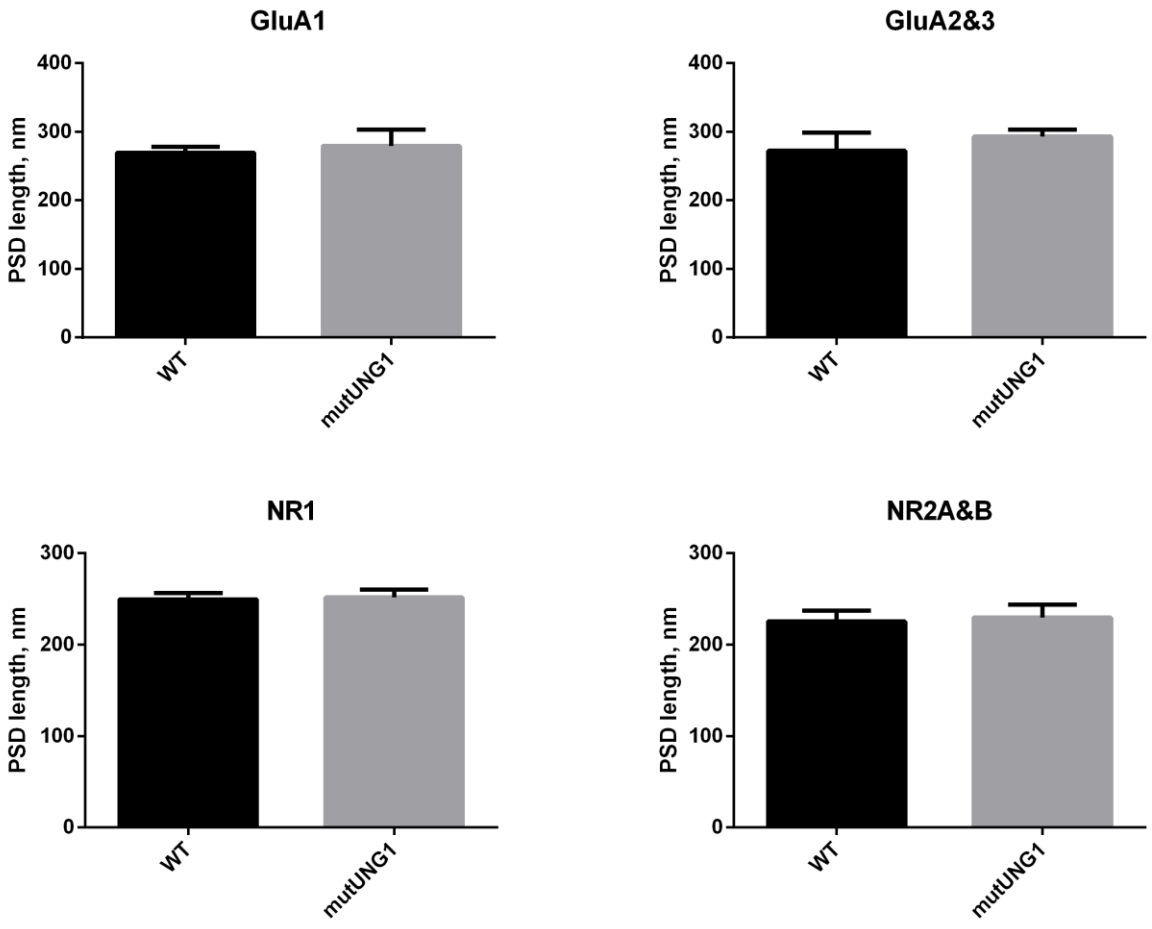

Figure 3.6 A graphical representation of the PSD length measured in wild type and mutUNG1 expressing mice showing immunogold labelling. There was found no significant difference. The PSD length of synapses labelled with antibodies for AMPA receptor subunits proved to be longer than the PSD length of synapses labelled with antibodies for NMDA receptor subunits.

Number of gold particles in wild type and mutUNG1 expressing mice			
Antibody	**Group**	**Gold particles**	***P*-value**
anti-GluA1	Wild type	1.35	0.37
	mutUNG1	1.30	
anti-Glua2&3	Wild type	3.44	0.40
	mutUNG1	3.20	
anti-NR1	Wild type	1.73	0.75
	mutUNG1	1.78	
anti-NR2A&B	Wild type	1.50	0.19
	mutUNG1	1.60	

Table 3.1 The number of gold particles recorded in synapses of wild type and mutUNG1 expressing mice. No statistical significance was observed as all *P*-values were higher than 0.05.

PSD length of wild type and mutUNG1 expressing mice			
Antibody	**Group**	**PSD length, nm**	***P*-value**
anti-GluA1	Wild type	270	0.39
	mutUNG1	279	
anti-Glua2&3	Wild type	272	0.13
	mutUNG1	293	
anti-NR1	Wild type	250	0.67
	mutUNG1	252	
anti-NR2A&B	Wild type	225	0.56
	mutUNG1	230	

Table 3.2 The PSD lengths of wild type and mutUNG1 expressing mice. No statistical significance was observed as all *P*-values were higher than 0.05.

4 Discussion of methods

4.1 Mouse as a model organism

Mouse is a popular model organism used to study biological phenomena like gene function and diseases. It fulfills many of the criteria that a model organism should have, like size, a short generation time and production of many offspring. Mouse is a mammal and not far away, seen on an evolutionary timescale, from humans. We share almost the same set of genes and have very similar physiology and anatomy. The hippocampus is for example very similar between the species, although smaller in mice.

Transgenic mice are genetically modified by adding foreign DNA into their genome, like was done for the creation of the mutUNG1 heart failure mouse (Lauritzen et al., 2014). The mouse was originally designed to study the effect of mitochondrial dysfunction in myocardiocytes, but it also allowed for the study of how a dysfunctional heart might affect the brain.

4.2 Number of experimental animals

The number of animals has an impact on the statistical data. Two groups of three mice in each (3 WT mice + 3 mutUNG1 mice) were used for the relative quantification of gene expression by qPCR. This is too few to assume a normalization of the data, and the student's *t*-test is therefore not usable. The Mann-Whitney U-test was therefore used as this test does not assume normalization. More animals will be needed to ensure confidence in the data. The data obtained were for that reason considered more as an indication.

Two groups of six mice in each (6 WT mice + 6 mutUNG1 mice) were used for analyzing differences in glutamate receptor subunit expression at the protein level and PSD diameter by postembedding immunogold electron microscopy. The number of animals here was considered as sufficient for doing the student's *t*-test on the data acquired.

4.3 Quantitative polymerase chain reaction (qPCR)

SYBR green is a fluorescent dye that binds double-stranded DNA (dsDNA) with great affinity. The increase in fluorescence is linear to the increase of DNA being amplified, making it a convenient tool for detection of PCR products. It can detect as few as 1-10 copies of a gene of interest. However, its advantage is also its disadvantage. The property of binding all dsDNA involves the risk of false positives if the sample is contaminated with unwanted DNA. Good and specific primers are therefore important to avoid primer-dimers and to ensure that only the gene of interest is amplified.

No template controls were included to check for contamination, but also for primer-dimers. As cDNA is the only kind of DNA of interest here, the presence of genomic DNA (gDNA) is therefore unwanted. Presence of gDNA can be a problem if it contains pseudogenes with sequences complementary to the primers being used. The isolated RNA was therefore treated with DNase, an enzyme that degrades DNA, to prevent any DNA that might have been transferred along with the RNA from being amplified during qPCR. It should be mentioned that the qPCR setups did not include any -RT controls. A -RT control is made during the RT-PCR setup by adding all reagents, but not the reverse transcriptase. After RT-PCR, it should therefore not contain any DNA as the RNA is not converted to cDNA. The solution is then used as -RT controls during qPCR. If the -RT control yields a fluorescent signal, it indicates a possible presence of gDNA. The lack of -RT controls must be considered a weakness of the qPCR setup used in this study, even though the presence of gDNA is very unlikely as the RNA was DNase-treated. The RNA was also checked for suspicious bands on an agarose gel and did not show any (figure 3.1).

The standard curve method was, as previously mentioned, chosen as the method for analyzing the data. The standard curve method requires the least amount of optimization and validation compared to other methods. The most critical steps during setup are accurate dilution of samples and the pipetting when adding template to the SYBR green mixture. The latter was experienced to be particularly important when adding the most diluted template to the standard curves, as slight variances easily ruin the standard curve, making it unusable.

GAPDH, β-Actin and 18S rRNA are popular reference genes as they are housekeeping genes

and should be stably expressed across all the samples. However, induced mutations might affect the gene expression, and it is therefore important to validate the expression levels before choosing a reference gene to go with (Kozera and Rapacz, 2013). Expression of GAPDH was clearly affected in myocardiocytes of the mutUNG1 heart failure mouse model, showing different expression levels across the mice being used, and β-Actin was found to be a better reference gene (Lauritzen et al., 2014). GAPDH was however not affected in hippocampal tissue of the same mice. In addition to normalizing the data, it also serves as a control for pipetting errors and variances between the individual sample's RT-PCR efficiency.

4.4 Antibody specificity

Using unspecific antibodies involves the risk of false positives since the antibodies might bind to several proteins, and not only the protein of interest, sharing a similar epitope. Antibody specificity is therefore crucial when performing post-embedding immunogold labelling.

The specificity of primary antibodies was tested by western blotting. A specific antibody is expected to yield a single band on the immunoblot. However, it is difficult to avoid additional weaker bands completely as several factors can influence this, like too high protein and/or antibody concentrations, inefficient blocking and proteolytic breakdown of the antigen during homogenization. Anti-GluA1 and anti-GluA2&3 did show strong bands at the expected location and was assumed to be specific. Anti-NR2A&B did show one additional band, but this was thought to be a fragment, as this antibody has been proven specific by others before (Jensen et al., 2009).

It is generally of interest to avoid the use of antibodies from the same organism as the organismal tissue it will be used with. The NR1 antibody was made by mouse cells, but was chosen as no other usable antibody was found. In addition to the expected band, it did show some other bands. However, these bands got weaker when reducing the primary antibody concentration, while the expected band remained about the same. It was therefore presumed to be specific enough. A screening for the concentration to be used in the immunogold procedure was also performed, which did show labelling in the PSD and low background labelling.

As for the immunogold procedure, it should also be noted that proteins might be altered during fixation and embedding which may affect the specificity prior to incubation with antibodies (Amiry-Moghaddam and Ottersen, 2013). The freeze-embedding procedure with Lowicryl H2MO, however, preserves antigens to a greater degree compared to other embedding procedures (Bergersen et al., 2008).

The specificity of secondary antibodies was confirmed by negative controls. The negative controls are sections subjected to the same experimental protocol as the other sections, but without incubation in primary antibodies. The sections should not contain any gold particles when looking in the electron microscope since there should be no primary antibodies for the secondary antibodies to bind to.

4.5 Immunogold labelling efficiency

The labelling efficiency of the immunogold method is defined as the ratio between the number of gold particles and the number of antigens present in the tissue (Mathiisen et al., 2006). Several factors affect the labelling efficiency. Variations in the immunogold procedure, like antibody concentatrion, temperature fluctuations, rinsing and incubation time, will affect the efficiency, and is it therefore important that the sections to be compared have been treated as similarly as possible. Sections of wild type and mutUNG1 expressing mice, labelled with the same antibody, were therefore all included in the same run of the immunogold procedure.

The choice of fixation medium affects not only tissue morphology, but also the labelling efficiency. The fixation medium used was a combination of formaldehyde and glutaraldehyde. Glutaraldehyde is a stronger protein cross-linker than formaldehyde, due to having more aldehyde groups for binding to the amino groups of proteins (Kiernan, 2000). It this therefore used to better preserve tissue morphology, but it can lower antibody binding. A low concentration of glutaraldehyde in the fixative is necessary to prevent the immunogold signal from being quenched when labelling for membrane proteins.

The choice of embedding medium will also affect labelling efficiency. Embedding in resin is done to prevent shrinkage of the tissue and being strong enough for the ultrathin sections required for electron microscopy (Hobot and Newman, 1996). Antigens might bind to the resin during the embedding procedure and thus reducing the labelling efficiency. However, Lowicryl HM20, a water-insoluble acryl-based resin, results in superior immunogold sensitivity by preserving the antigens to a large extent (Campagne et al., 1991; Bergersen et al., 2008).

4.6 Background labelling

It is difficult to avoid unspecific of the background completely, despite the antibodies showing specificity on western blot, because of the postembedding protocol itself (Bergersen et al., 2008). Unspecific labelling of is typically seen in structures which contain a high density of proteins, like the mitochondrial membrane. Like with the labelling efficiency in general, the background labelling is also affected by the same variables. Two different blocking solutions were used to prevent non-specific labelling as much as possible. The protein and ion concentrations in the blocking solutions can also be adjusted to affect labelling.

4.7 Quantification of gold particles

The colloidal gold particles used for post-embedding immunogold labelling are electron dense and can be seen at high magnification in the electron microscope. Even though electron microscopy yields a very high resolution, the lateral resolution of the immunogold procedure must be taken into account when analyzing the micrographs. The diameter of the gold particles used in this study was 10 nm, making the distance from the gold particle to the epitope approximately 25 nm (figure 2.3b). Gold particles located 25 nm away on either side of the postsynaptic membrane (in the PSD region) were therefore recorded.

An advantage with the immunogold procedure is the equal probability of antibody binding to antigens on the section surface. It is should be noted that the amount of gold particles does not equal the number of antigens present in the tissue (Amiry-Moghaddam and Ottersen, 2013).

This is because of the previously mentioned factors affecting the labelling efficiency. However, there is an approximately linear relationship between the number of gold particles and available antigens (Ottersen, 1989). The amount of labelling can therefore be used to quantify the number of antigens present in the tissue. However, it is important to remember that the quantification is not absolute.

5 Discussion of results

5.1 Gene expression

The data obtained by qPCR showed there was a variable expression of mRNA for AMPA and NMDA receptor subunit within the two groups. This variance made it difficult to observe any difference, especially when working with a small sample size due to it being extra sensitive to variations within the data. The Mann-Whitney *U* test showed no significant difference for all the genes that were analyzed.

Not all receptor subunits were analyzed. These include GluA4, NR2C and NR3B. CA1 pyramidal neurons express AMPA receptors consisting mainly of GluA2 subunits in combination with either GluA3, but also GluA1 (Andersen et al., 2007, p. 254). NR2C is not significantly expressed in the adult hippocampus, and NR3B is not expressed at all.

5.2 Immunogold electron microscopy

The data obtained by immunogold labelling in combination with electron microscopy did not reveal any difference. However, the variance observed by qPCR was not found to be reflected at the protein level. The number of glutamate receptor subunits was very much the same in both groups. This was also the case for the PSD lengths.

The average PSD lengths of those synapses that were labelled for AMPA receptor subunits were longer than the average PSD lengths of the synapses that were labelled for NMDA receptor subunits. This is in accordance with a previous study that showed a difference in PSD lengths of synapses containing only NMDA receptors (silent synapses) compared to synapses containing both NMDA and AMPA receptors in the Schaffer collateral pathway (Takumi et al., 1999). They did also show that the ratio of AMPA to NMDA is a linear function of the PSD length, and that AMPA receptor number drops to zero in PSDs shorter

than ~180 nm. It could be speculated that this is a consequence of LTP, where the insertion of AMPA receptors leads to a bigger PSD.

Analysis of synapses did only include those synapses that showed immunogold labelling in their PSDs. There could be a difference in the number of synapses containing glutamate receptors if non-labelled synapses were included in the analysis. This means that a total change in the number of AMPA and NMDA receptors and/or receptor subunits cannot be excluded.

An increase in the number of silent synapses is also possible. To investigate these synapses would require the sections to be labelled with two different antibodies (with different gold particle diameter for being able to visually separate the two), preferably against NR1 and GluA2 as these subunits are included in all AMPA and NMDA receptors in Schaffer collateral-CA1 synapses.

5.3 Conclusion

1. Variations in gene expression of AMPA and NMDA receptor subunits in the hippocampus were found in both groups of mutUNG1 expressing and wild type mice. However, no significant difference was found when comparing the two groups.

2. No alterations in the number of AMPA and NMDA receptors and/or subunit composition were found in excitatory synapses of Schaffer collateral-CA1 synapses when comparing mutUNG1 expressing to wild type mice.

3. No alterations in PSD length of Schaffer collateral-CA1 synapses containing immunogold labelling were found when comparing mutUNG1 expressing to wild type mice. The PSD length of synapses labelled for AMPA receptor subunits were longer than those labelled for NMDA receptor subunits.

The mutUNG1 expressing mouse model was originally created to study how mitochondrial dysfunction affects the cardiomyocytes of the heart. Average life expectancy after induction of mutUNG1 expression is approximately two months before they die of cardiac arrest. Even though no changes were observed when studying the brain of these mice, the possibility that such a short time period is not enough to affect the brain exists. The use of other animal models of cardiac dysfunction with a longer life expectancy might be better suited to show any consequences on brain function. Actually, in another study using a heart failure mouse model it was shown moderate impairment in spatial learning tasks in the Morris water maze (Hong et al., 2013). This moderate impairment was observed after three months of chronic HF, suggesting that the average life expectancy of two months of the mutUNG1 expressing mouse model is not a sufficient period of time for the HF condition to affect the brain. In addition, alterations in other brain areas cannot be ruled out.

References

Abraham, W.C., Logan, B., Greenwood, J.M., Dragunow, M., 2002. Induction and experience-dependent consolidation of stable long-term potentiation lasting months in the hippocampus. J. Neurosci. Off. J. Soc. Neurosci. 22, 9626–9634.

Abraham, W.C., Williams, J.M., 2003. Properties and mechanisms of LTP maintenance. Neurosci. Rev. J. Bringing Neurobiol. Neurol. Psychiatry 9, 463–474.

Amiry-Moghaddam, M., Ottersen, O.P., 2013. Immunogold cytochemistry in neuroscience. Nat. Neurosci. 16, 798–804.

Andersen, P., Morris, R., Amaral, D., Bliss, T., O'Keefe, J., 2007. The Hippocampus Book. Oxford University Press.

Ankarcrona, M., Dypbukt, J.M., Bonfoco, E., Zhivotovsky, B., Orrenius, S., Lipton, S.A., Nicotera, P., 1995. Glutamate-induced neuronal death: A succession of necrosis or apoptosis depending on mitochondrial function. Neuron 15, 961–973.

Arundine, M., Tymianski, M., 2003. Molecular mechanisms of calcium-dependent neurodegeneration in excitotoxicity. Cell Calcium, Neuronal Calcium Toxicity 34, 325–337.

Axmacher, N., Elger, C.E., Fell, J., 2009. Working Memory-Related Hippocampal Deactivation Interferes with Long-Term Memory Formation. J. Neurosci. 29, 1052–1060.

Barth, E., Stämmler, G., Speiser, B., Schaper, J., 1992. Ultrastructural quantitation of mitochondria and myofilaments in cardiac muscle from 10 different animal species including man. J. Mol. Cell. Cardiol. 24, 669–681.

Ben-Yakov, A., Dudai, Y., 2011. Constructing realistic engrams: poststimulus activity of hippocampus and dorsal striatum predicts subsequent episodic memory. J. Neurosci. Off. J. Soc. Neurosci. 31, 9032–9042.

Bergersen, L.H., Storm-Mathisen, J., Gundersen, V., 2008. Immunogold quantification of amino acids and proteins in complex subcellular compartments. Nat. Protoc. 3, 144–152.

Campagne, M. van L., Oestreicher, A.B., Krift, T.P. van der, Gispen, W.H., Verkleij, A.J., 1991. Freeze-substitution and Lowicryl HM20 embedding of fixed rat brain: suitability for immunogold ultrastructural localization of neural antigens. J. Histochem. Cytochem. 39, 1267–1279.

Carta, M., Fièvre, S., Gorlewicz, A., Mulle, C., 2014. Kainate receptors in the hippocampus. Eur. J. Neurosci.

Cull-Candy, S.G., Leszkiewicz, D.N., 2004. Role of distinct NMDA receptor subtypes at central synapses. Sci. STKE Signal Transduct. Knowl. Environ. 2004, re16.

Dardiotis, E., Giamouzis, G., Mastrogiannis, D., Vogiatzi, C., Skoularigis, J., Triposkiadis, F., Hadjigeorgiou, G.M., 2012. Cognitive Impairment in Heart Failure. Cardiol. Res. Pract. 2012, e595821.

De la Torre, J.C., 2004. Is Alzheimer's disease a neurodegenerative or a vascular disorder? Data, dogma, and dialectics. Lancet Neurol. 3, 184–190.

Derkach, V., Barria, A., Soderling, T.R., 1999. Ca2+/calmodulin-kinase II enhances channel conductance of α-amino-3-hydroxy-5-methyl-4-isoxazolepropionate type glutamate receptors. Proc. Natl. Acad. Sci. 96, 3269–3274.

Eichenbaum, H., 2013. What H.M. Taught Us. J. Cogn. Neurosci. 25, 14–21.

Falkenberg, M., Larsson, N.-G., Gustafsson, C.M., 2007. DNA replication and transcription in mammalian mitochondria. Annu. Rev. Biochem. 76, 679–699.

Friedman, J.R., Nunnari, J., 2014. Mitochondrial form and function. Nature 505, 335–343.

Gundersen, V., Danbolt, N.C., Ottersen, O.P., Storm-Mathisen, J., 1993. Demonstration of glutamate/aspartate uptake activity in nerve endings by use of antibodies recognizing exogenous D-aspartate. Neuroscience 57, 97–111.

Hafting, T., Fyhn, M., Molden, S., Moser, M.-B., Moser, E.I., 2005. Microstructure of a spatial map in the entorhinal cortex. Nature 436, 801–806.

Hayashi, Y., Shi, S.H., Esteban, J.A., Piccini, A., Poncer, J.C., Malinow, R., 2000. Driving AMPA receptors into synapses by LTP and CaMKII: requirement for GluR1 and PDZ domain interaction. Science 287, 2262–2267.

Hobot, J.A., Newman, G.R., 1996. Immunomicroscopy: resin techniques and on-section labelling with immunocolloidal gold or immunoperoxidase--planning a protocol. Scanning Microsc. 10, 121–143; discussion 143–145.

Hong, X., Bu, L., Wang, Y., Xu, J., Wu, J., Huang, Y., Liu, J., Suo, H., Yang, L., Shi, Y., Lou, Y., Sun, Z., Zhu, G., Behnisch, T., Yu, M., Jia, J., Hai, W., Meng, H., Liang, S., Huang, F., Zou, Y., Ge, J., 2013. Increases in the risk of cognitive impairment and alterations of cerebral β-amyloid metabolism in mouse model of heart failure. PloS One 8, e63829.

Isaac, J.T., Nicoll, R.A., Malenka, R.C., 1995. Evidence for silent synapses: implications for the expression of LTP. Neuron 15, 427–434.

Jensen, V., Rinholm, J.E., Johansen, T.J., Medin, T., Storm-Mathisen, J., Sagvolden, T., Hvalby, O., Bergersen, L.H., 2009. N-methyl-D-aspartate receptor subunit dysfunction at hippocampal glutamatergic synapses in an animal model of attention-deficit/hyperactivity disorder. Neuroscience 158, 353–364.

Kandel, E.R., Schwartz, J.H., Jessell, T.M., Siegelbaum, S.A., Hudspeth, A.J., 2012. Principles of Neural Science, 5th edition. ed. McGraw-Hill Professional.

Kentros, C., Hargreaves, E., Hawkins, R.D., Kandel, E.R., Shapiro, M., Muller, R.V., 1998. Abolition of Long-Term Stability of New Hippocampal Place Cell Maps by NMDA Receptor Blockade. Science 280, 2121–2126.

Kiernan, J.A., 2000. Formaldehyde, formalin, paraformaldehyde, and glutaraldehyde: What they are and what they do. Microsc. Today 8, 8–12.

Kovalenko, T., Osadchenko, I., Nikonenko, A., Lushnikova, I., Voronin, K., Nikonenko, I., Muller, D., Skibo, G., 2006. Ischemia-induced modifications in hippocampal CA1 stratum radiatum excitatory synapses. Hippocampus 16, 814–825.

Kozera, B., Rapacz, M., 2013. Reference genes in real-time PCR. J. Appl. Genet. 54, 391–406.

Laake, J.H., Slyngstad, T.A., Haug, F.M., Ottersen, O.P., 1995. Glutamine from glial cells is essential for the maintenance of the nerve terminal pool of glutamate: immunogold evidence from hippocampal slice cultures. J. Neurochem. 65, 871–881.

Lauritzen, K.H., Kleppa, L., Aronsen, J.M., Eide, L., Carlsen, H., Haugen, Ø.P., Sjaastad, I., Klungland, A., Storm-Mathisen, J., Juel Rasmussen, L., Attramadal, H., Bergersen, L.H., 2014. Impaired dynamics and function of mitochondria caused by mtDNA toxicity leads to heart failure. Manuscript submitted for publication.

Lee, C.-W., Shih, Y.-H., Kuo, Y.-M., 2014. Cerebrovascular pathology and amyloid plaque formation in Alzheimer's disease. Curr. Alzheimer Res. 11, 4–10.

Lindahl, T., Wood, R.D., 1999. Quality control by DNA repair. Science 286, 1897–1905.

Lisman, J., 1989. A mechanism for the Hebb and the anti-Hebb processes underlying learning and memory. Proc. Natl. Acad. Sci. 86, 9574–9578.

Lüscher, C., Malenka, R.C., 2012. NMDA receptor-dependent long-term potentiation and long-term depression (LTP/LTD). Cold Spring Harb. Perspect. Biol. 4.

Mathiisen, T.M., Nagelhus, E.A., Jouleh, B., Torp, R., Frydenlund, D.S., Mylonakou, M.-N., Amiry-Moghaddam, M., Covolan, L., Utvik, J.K., Riber, B., Gujord, K.M., Knutsen, J., Skare, Ø., Laake, P., Davanger, S., Haug, F.-M., Rinvik, E., Ottersen, O.P., 2006. Postembedding Immunogold Cytochemistry of Membrane Molecules and Amino Acid Transmitters in the Central Nervous System, in: Zaborszky, L., Wouterlood, F.G., Lanciego, J.L. (Eds.), Neuroanatomical Tract-Tracing 3. Springer US, pp. 72–108.

McHugh, T.J., Blum, K.I., Tsien, J.Z., Tonegawa, S., Wilson, M.A., 1996. Impaired Hippocampal Representation of Space in CA1-Specific NMDAR1 Knockout Mice. Cell 87, 1339–1349.

Monyer, H., Burnashev, N., Laurie, D.J., Sakmann, B., Seeburg, P.H., 1994. Developmental and regional expression in the rat brain and functional properties of four NMDA receptors. Neuron 12, 529–540.

Naito, S., Ueda, T., 1983. Adenosine triphosphate-dependent uptake of glutamate into protein I-associated synaptic vesicles. J. Biol. Chem. 258, 696–699.

Neves, G., Cooke, S.F., Bliss, T.V.P., 2008. Synaptic plasticity, memory and the hippocampus: a neural network approach to causality. Nat. Rev. Neurosci. 9, 65–75.

Newman, M.F., Kirchner, J.L., Phillips-Bute, B., Gaver, V., Grocott, H., Jones, R.H., Mark, D.B., Reves, J.G., Blumenthal, J.A., Neurological Outcome Research Group and the Cardiothoracic Anesthesiology Research Endeavors Investigators, 2001. Longitudinal assessment of neurocognitive function after coronary-artery bypass surgery. N. Engl. J. Med. 344, 395–402.

Nilsen, H., Otterlei, M., Haug, T., Solum, K., Nagelhus, T.A., Skorpen, F., Krokan, H.E., 1997. Nuclear and mitochondrial uracil-DNA glycosylases are generated by alternative splicing and transcription from different positions in the UNG gene. Nucleic Acids Res. 25, 750–755.

Nilsen, H., Steinsbekk, K.S., Otterlei, M., Slupphaug, G., Aas, P.A., Krokan, H.E., 2000. Analysis of uracil-DNA glycosylases from the murine Ung gene reveals differential expression in tissues and in embryonic development and a subcellular sorting pattern that differs from the human homologues. Nucleic Acids Res. 28, 2277–2285.

O'Keefe, J., Nadel, L., 1978. The Hippocampus as a Cognitive Map. Oxf. Univ. Press.

Otterlei, M., Haug, T., Nagelhus, T.A., Slupphaug, G., Lindmo, T., Krokan, H.E., 1998. Nuclear and mitochondrial splice forms of human uracil-DNA glycosylase contain a complex nuclear localisation signal and a strong classical mitochondrial localisation signal, respectively. Nucleic Acids Res. 26, 4611–4617.

Ottersen, O.P., 1989. Postembedding immunogold labelling of fixed glutamate: an electron microscopic analysis of the relationship between gold particle density and antigen concentration. J. Chem. Neuroanat. 2, 57–66.

Pellegrini-Giampietro, D.E., Zukin, R.S., Bennett, M.V., Cho, S., Pulsinelli, W.A., 1992. Switch in glutamate receptor subunit gene expression in CA1 subfield of hippocampus following global ischemia in rats. Proc. Natl. Acad. Sci. U. S. A. 89, 10499–10503.

Schmidt-Kastner, R., Freund, T.F., 1991. Selective vulnerability of the hippocampus in brain ischemia. Neuroscience 40, 599–636.

Scoville, W.B., Milner, B., 1957. Loss of Recent Memory After Bilateral Hippocampal Lesions. J. Neurol. Neurosurg. Psychiatry 20, 11–21.

Seeburg, P.H., Burnashev, N., Köhr, G., Kuner, T., Sprengel, R., Monyer, H., 1995. The NMDA receptor channel: molecular design of a coincidence detector. Recent Prog. Horm. Res. 50, 19–34.

Slupphaug, G., Markussen, F.H., Olsen, L.C., Aasland, R., Aarsaether, N., Bakke, O., Krokan, H.E., Helland, D.E., 1993. Nuclear and mitochondrial forms of human uracil-DNA glycosylase are encoded by the same gene. Nucleic Acids Res. 21, 2579–2584.

Smith, C.N., Squire, L.R., 2009. Medial temporal lobe activity during retrieval of semantic memory is related to the age of the memory. J. Neurosci. Off. J. Soc. Neurosci. 29, 930–938.

Smith, D.M., Mizumori, S.J.Y., 2006. Hippocampal place cells, context, and episodic memory. Hippocampus 16, 716–729.

Sommer, B., Köhler, M., Sprengel, R., Seeburg, P.H., 1991. RNA editing in brain controls a determinant of ion flow in glutamate-gated channels. Cell 67, 11–19.

Sugawara, T., Fujimura, M., Morita-Fujimura, Y., Kawase, M., Chan, P.H., 1999. Mitochondrial release of cytochrome c corresponds to the selective vulnerability of hippocampal CA1 neurons in rats after transient global cerebral ischemia. J. Neurosci. Off. J. Soc. Neurosci. 19, RC39.

Takahashi, M., Sarantis, M., Attwell, D., 1996. Postsynaptic glutamate uptake in rat cerebellar Purkinje cells. J. Physiol. 497 (Pt 2), 523–530.

Takumi, Y., Ramírez-León, V., Laake, P., Rinvik, E., Ottersen, O.P., 1999. Different modes of expression of AMPA and NMDA receptors in hippocampal synapses. Nat. Neurosci. 2, 618–624.

Tang, Y.-P., Shimizu, E., Dube, G.R., Rampon, C., Kerchner, G.A., Zhuo, M., Liu, G., Tsien, J.Z., 1999. Genetic enhancement of learning and memory in mice. Nature 401, 63–69.

Tovar, K.R., McGinley, M.J., Westbrook, G.L., 2013. Triheteromeric NMDA receptors at hippocampal synapses. J. Neurosci. Off. J. Soc. Neurosci. 33, 9150–9160.

Traynelis, S.F., Wollmuth, L.P., McBain, C.J., Menniti, F.S., Vance, K.M., Ogden, K.K., Hansen, K.B., Yuan, H., Myers, S.J., Dingledine, R., 2010. Glutamate receptor ion channels: structure, regulation, and function. Pharmacol. Rev. 62, 405–496.

Tulving, E. Episodic and semantic memory.. In: Tulving, E.; Donaldson, W., editors. Organization of memory. Academic Press; New York: 1972. p. 381-403.

Vogels, R.L.C., Oosterman, J.M., van Harten, B., Scheltens, P., van der Flier, W.M., Schroeder-Tanka, J.M., Weinstein, H.C., 2007a. Profile of cognitive impairment in chronic heart failure. J. Am. Geriatr. Soc. 55, 1764–1770.

Vogels, R.L.C., Scheltens, P., Schroeder-Tanka, J.M., Weinstein, H.C., 2007b. Cognitive impairment in heart failure: a systematic review of the literature. Eur. J. Heart Fail. 9, 440–449.

Zhu, H., Yoshimoto, T., Imajo-Ohmi, S., Dazortsava, M., Mathivanan, A., Yamashima, T., 2012. Why are hippocampal CA1 neurons vulnerable but motor cortex neurons resistant to transient ischemia? J. Neurochem. 120, 574–585.

Appendices

Appendix A – Reagents and chemicals

Chemical name	Molecular formula	Manufacturer
Acetate	CH_3CO_2H	Sigma-Aldrich, USA
Agarose	$C_{24}H_{38}O_{19}$	Sigma-Aldrich, USA
Bovine serum albumine		Fluka Chemica, Switzerland
Bromophenol blue	$C_{19}H_{10}Br_4O_5S$	Sigma-Aldrich, USA
Chloroform	$CHCl_3$	Sigma-Aldrich, USA
Disodium phosphate	Na_2HPO_4	Sigma-Aldrich, USA
Dithioerythritol	$HSCH_2CH(OH)CH(OH)CH_2SH$	Sigma-Aldrich, USA
Ethanol	EtOH	Arcus Kjemi AS, Norway
Ethidium bromide	$C_{21}H_{20}BrN_3$	Sigma-Aldrich, USA
Ethylenediaminetetraacetic acid	$C_{10}H_{16}N_2O_8$	Electron Microscopic Services, USA
Glycine	$C_2H_5NO_2$	Sigma-Aldrich, USA
Human serum albumin		Sigma-Aldrich, USA
Hydrogen peroxide	H_2O_2	Fluka Chemica, Switzerland
Isopropanol	$(CH_3)_2CHOH$	Sigma-Aldrich, USA
Lead citrate	$Pb_3(C_6H_5O_7)_2$	The British Drug Houses Ltd, Great Britain
Nonidet-P40	$(C_2H_4O)nC_{14}H_{22}O$	Sigma-Aldrich, USA
Polyethylene glycol	$C_{15}H_{16}O_2{\cdot}C_3H_5ClO{\cdot}(C_2H_4O)n{\cdot}H_2O]x$	Sigma-Aldrich, USA
Protease inhibitor cocktail		Sigma-Aldrich, USA
Sodium borohydride	$NaBH_4$	Fluka Chemica, Switzerland
Sodium chloride	NaCl	Fluka Chemica, Switzerland
Sodium deoxycholate	$C_{24}H_{39}NaO_4$	Sigma-Aldrich, USA
Sodium dihydrogen phosphate	NaH_2PO_4	Sigma-Aldrich, USA
Sodium dodecyl sulfate	$NaC_{12}H2_5SO_4$	Fluka Chemica, Switzerland
Sodium hydroxide (2 M)	NaOH	Electron Microscopic

		Services, USA
Triton X-100	$C_{14}H_{22}O(C_2H_4O)n$ (n=9-10)	Sigma-Aldrich, USA
Trizma base	$NH_2C(CH_2OH)_3$	Sigma-Aldrich, USA
Trizma hydrochloride	$NH_2C(CH_2OH)_3 \cdot HCl$	Sigma-Aldrich, USA
Tween 20	$C_{58}H_{114}O_{26}$	Fluka Chemica, Switzerland
Uranyl acetate	$UO_2(CH_3COO)_2$	Fluka Chemica, Switzerland

Appendix B – Solutions

Buffers

- **RIPA buffer:** 25 mM Trizma HCl pH 7.6, 150 mM NaCl, 1% NP40, 0.1% SDS, 0.5% Na deoxycholate and protease inhibitor cocktail (1 tablet). Store at 4 °C.

- **1% SDS buffer:** 2.3 mg disodium hydrogen phosphate (Na2HPO4), 0.46 g monosodium phosphate (NaH2PO4), 2 g SDS, 2 tablets of protease inhibitor cocktail. Mix in 200 ml MQ water.

- **TAE buffer (50X):** Mix 242 g Trizma base, 57.1 ml acetate and 100 ml of 0.5 M EDTA. Dilute 20 ml in 980 of MQ water for 1X TAE buffer.

- **Laemmli sample buffer (2X) w/ DTT:** 20 ml 87% glycerol, 12.5 ml 1 M Trizma HCl, 4 g SDS, few grains of bromophenol blue. Add MQ water up to 100 ml. Adjust pH to 6.8. Store at room temperature. Add 10 µl of DTT to 40 µl of Laemmli sample buffer (2X).
  - 0.5 M Dithioerythritol (DTT): 39 mg in 0,5 ml MQ water. Store at 4 °C for up to one week. DTT reduces the disulfide bonds of proteins.

- **Running buffer (10X):** 30.3 g 25mM Tris base, 144 g 192 mM glycine, 10 g SDS. Dissolve in 1 l of MQ water.

- **Blotting buffer (1X):** 3.03 g 25mM Tris base, 14.4 g 192 mM glycine, 100 ml 10% isopropanol. Dissolve in 1 l of MQ water.

- **Tris-buffered Saline w/ Tween (TBSTw):** 7.9 g 10 mM Trizma HCl, 43.8 g 150 mM NaCl, 2.5 ml 0.05% Tween 20. Dissolve in 5 l of MQ water.

- **0,1 M Phosphate buffer (PB):** Dissolve 11.5 g disodium phosphate (Na_2HPO_4) and 2.3 g sodium dihydrogen phosphate (NaH_2PO_4) in 1 L of MQ water. Adjust pH to 7.4.

- **0,05 M Tris buffer:** Dissolve 0.97 g Trizma base ($NH_2C(CH_2OH)_3$) and 6.61 Trizma HCl ($NH_2C(CH_2OH)_3HCl$) in 1 L of MQ water. Adjust pH to 7.4.

- **Tris Buffered Saline Triton (TBST):** Mix 100 ml 0.05 M Tris buffer, 900 ml 0.3% NaCl and 1 ml Triton X-100-0.1%.
  - 0.3% NaCl: Dissolve 3 g NaCl in 1 L of MQ water.

Etching solution

- **2% Hydrogen Peroxide (immunogold):** Mix 40 µl 30% H_2O_2 with 560 mL of PB.

Blocking solutions

- **4% Bovine Serum Albumin (Western blot):** Dissolve 4 g of BSA in 100 ml of TBSTw. Make fresh before each procedure.

- **1% Bovine Serum Albumin (Western blot):** Dissolve 1 g of BSA in 100 ml of TBSTw. Make fresh before each procedure.

- **Borohydride/Glycine solution (immunogold):** Dissolve 37 mg glycine and 10 mg Na-borohydride in 10 ml of TBST. Make fresh before each procedure.

- **2% Human serum albumin (immunogold):** Dissolve 60 mg HSA in 3 ml TBST. Make fresh before each procedure.

- **2% Human serum albumin w/ PEG (immunogold):** Add 25 mg polyethylene glycol (PEG) to 50 ml of TBST. Store at 4 °C. Dissolve 60 mg HSA in 3 ml of this TBST w/ PEG. Make fresh before each procedure.

Contrasting solutions

- **1% Uranyl acetate (immunogold):** The reagents needed for this solution are toxic and must therefore be mixed in a fume hood. Mix 5 g of uranyl acetate and 40 ml of ethanol with 60 ml of pre-boiled MQ water. Cover the solution and place it on an electric shaker for the uranyl acetate to dissolve completely. Filter the solution and store at 4 °C in the dark.

- **0.3% Lead citrate (immunogold):** This must be carried out in a fume hood in order to protect the solution from CO_2, which otherwise may cause precipitation. Mix 0.15 g of lead citrate with 48 ml of pre-boiled MQ water. Add 2.5 ml of 2 M sodium hydroxide and place the solution on a magnetic stirrer plate. After sufficient mixing transfer the solution to an airtight container and store at 4 °C.

Appendix C – Kits

- **RNeasy Lipid Tissue Mini Kit** (QIAGEN, Netherlands): Contains mini spin columns, collection tubes, buffers, RNase-free water and QIAzol Lysis Reagent (contains phenol/guanidine, optimized for lysis of fatty tissue).

- **High Capacity RNA-to-cDNA kit** (Applied Biosystems, USA): Contains 20X Enzyme mix (MuLV and RNase inhibitor protein and 2X RT Buffer Mix (includes dNTPs, random octamers, and oligo dT-16).

- **SYBR® Green PCR Master Mix** (Applied Biosystems, USA): contains SYBR Green 1 Dye, AmpliTaq Gold® DNA Polymerase, dNTPs with dUTP, Passive Reference 1, and optimized buffer components.

- **BCA Protein Assay Kit** (Pierce, Thermo Scientific, USA): Contains BCA reagent A (bicinchoninic acid and sodium cabonate), BCA reagent B (cupric (II) sulfate) and bovine serum albumin standards.

- **SuperSignal® West Dura Extended Duration Substrate kit** (Pierce, Thermo Scientific, USA): luminol-based enhanced chemiluminescence (ECL) HRP substrate

Appendix D – Antibodies

PRIMARY ANTIBODIES

Antibody	Host	Class	Type	Antigen	Application	Company	Catalogue#	Lot #
Anti-GluA1	Rabbit	IgG	Polyclonal	Cytoplasmic site of the receptor	WB, EM	Millipore	AB1504	LV1519 2215
Anti-GluA2&3	Rabbit	IgG	Polyclonal	C-terminus	WB, EM	Millipore	AB1506	LV1583 031
Anti-NR1	Mouse	IgG	Monoclonal	Extracellular loop between transmembrane regions III & IV	WB, EM	Millipore	MAB363	2219311
Anti-NR2A&B	Rabbit	IgG	Polyclonal	C-terminus	WB, EM	Millipore	AB1548	LV1488 6500

SECONDARY ANTIBODIES

Antibody	Host	Class	Type	Antigen	Application	Company	Catalogue#	Lot #
ECL™ Anti-rabbit IgG, HRP-linked	Donkey	IgG	Polyclonal	Rabbit IgG	WB	GE Healthcare	NA934	337576
Anti-mouse IgG – Peroxidase	Rabbit	IgG	Polyclonal	Mouse IgG	WB	Sigma-Aldrich	A9044	010M4797
Anti Rabbit IgG 10nm Gold	Goat	$F(ab)_2$	Polyclonal	Rabbit IgG	EM	BBI Solutions	EM GFAR10	15617
Anti Mouse IgG Fc Specific 10nm Gold	Goat	IgG	Polyclonal	Mouse IgG Fc	EM	BBI Solutions	EM GAM10	14712

Appendix E – qPCR data

	GluA1	
Wild type (ID #)	**Normalized value**	**Average**
6	0.154577	
33	0.119011	0.162816
39	0.214858	
mutUNG1 (ID #)	**Normalized value**	**Average**
4	0.114341	
98	0.080788	0.100295
42	0.105756	

	GluA2	
Wild type (ID #)	**Normalized value**	**Average**
6	1.089693	
33	0.650834	1.020089
39	1.319742	
mutUNG1 (ID #)	**Normalized value**	**Average**
4	0.86882	
98	0.821434	0.906244
42	1.028479	

	GluA3	
Wild type (ID #)	**Normalized value**	**Average**
6	1.232039	
33	1.68329	1.508236
39	1.609379	
mutUNG1 (ID #)	**Normalized value**	**Average**
4	1.004668	
98	2.504993	1.82057
42	1.952049	

	NR1	
Wild type (ID #)	**Normalized value**	**Average**
6	0.938058	
33	0.837948	0.930265
39	1.01479	
mutUNG1 (ID #)	**Normalized value**	**Average**
4	0.617164	
98	0.685691	0.889565
42	1.36584	

	NR2A	
Wild type (ID #)	**Normalized value**	**Average**
6	1.221483	
33	0.875489	1.182984
39	1.45198	
mutUNG1 (ID #)	**Normalized value**	**Average**
4	0.677222	
98	0.465993	0.754718
42	1.120939	

	NR2B	
Wild type (ID #)	**Normalized value**	**Average**
6	0.093228	
33	0.104514	0.108537
39	0.127976	
mutUNG1 (ID #)	**Normalized value**	**Average**
4	0.028526	
98	0.09969	0.088955
42	0.138649	

	NR2D	
Wild type (ID #)	**Normalized value**	**Average**
6	0.076323	
33	0.102965	0.081953
39	0.066571	
mutUNG1 (ID #)	**Normalized value**	**Average**
4	0.027063	
98	0.081893	0.064693
42	0.085123	

	NR3A	
Wild type (ID #)	**Normalized value**	**Average**
6	0.921028	
33	1.372871	1.13708
39	1.117343	
mutUNG1 (ID #)	**Normalized value**	**Average**
4	0.356473	
98	1.369994	0,956055
42	1.141697	

Appendix F – Protein quantification

Absorbance measured at 562 nm

Protein, µg/ml	Abs.	Abs.	Abs.	Abs.
0	0.125	0.114	0.116	0.145
20	0.171	0.160	0.160	0.192
100	0.208	0.201	0.197	0.225
250	0.316	0.298	0.316	0.335
500	0.463	0.498	0.438	0.452
750	0.596	0.596	0.587	0.604
1000	0.736	0.748	0.726	0.735
2000	1.188	1.097	1.257	1.211

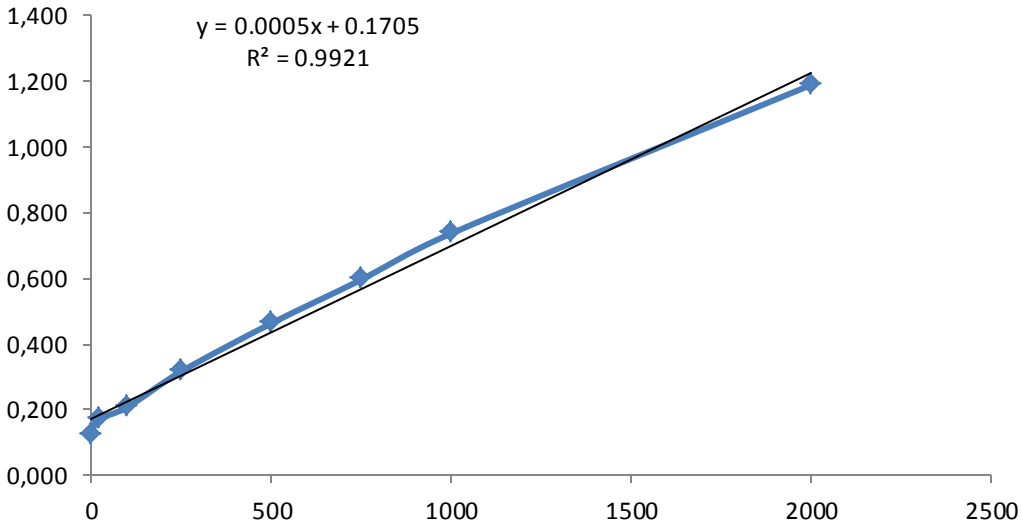

Dilution of protein homogenate with 1% SDS buffer	Abs.	Abs.	Abs.	Abs.	Protein in hom.	ug/ul in hom.
1:5 ->	1.747	1.741	1.718	1.781	3152.33	15.76
1:10 ->	1.041	1.034	1.045	1.045	1741.67	17.42
1:20 ->	0.688	0.663	0.723	0.678	1035	20.70

Average: 18 ug/ul

Dilution of protein homogenate for SDS-PAGE:
Dilute prot. hom. 1:9 with sample buffer to obtain a final concentration 2 ug/ul.

Appendix G – Immunogold electron microscopy data

	WT 6233 n = 39 synapses		WT 6234 n = 45 synapses		WT 6235 n = 35 synapses	
	PSD length, nm	**Gold particles**	**PSD length, nm**	**Gold particles**	**PSD length, nm**	**Gold particles**
Average:	257.85	1.21	266.55	1.49	265.65	1.34
Standard deviation:	79.65	0.41	55.51	0.79	75.11	0.64
Average deviation:	57.63	0.33	45.70	0.65	59.06	0.51
Max:	556.58	2.00	386.74	4.00	440.91	3.00
Min:	106.57	1.00	160.80	1.00	147.89	1.00

	WT 6236 n = 44 synapses		WT 6237 n = 39 synapses		WT 6238 n = 47 synapses	
	PSD length, nm	**Gold particles**	**PSD length, nm**	**Gold particles**	**PSD length, nm**	**Gold particles**
Average:	280.95	1.25	277.70	1.31	268.84	1.51
Standard deviation:	90.59	0.58	65.19	0.73	78.25	1.06
Average deviation:	72.66	0.41	48.54	0.50	60.62	0.72
Max:	560.86	3.00	481.70	4.00	498.28	7.00
Min:	151.32	1.00	143.47	1.00	99.77	1.00

Table A.1 A summary of the synapses analyzed in wild type mice labeled with antibodies for GluA1.

	mutUNG1 6239 n = 38 synapses		mutUNG1 6240 n = 38 synapses		mutUNG1 6241 n = 44 synapses	
	PSD length, nm	**Gold particles**	**PSD length, nm**	**Gold particles**	**PSD length, nm**	**Gold particles**
Average:	320.48	1.26	247.09	1.24	270.52	1.32
Standard deviation:	93.51	0.55	62.71	0.59	63.76	0.64
Average deviation:	72.73	0.42	51.80	0.39	52.91	0.48
Max:	537.31	3.00	369.96	4.00	406.08	4.00
Min:	183.44	1.00	108.93	1.00	161.67	1.00

	mutUNG1 6242 n = 41 synapses		mutUNG1 6243 n = 39 synapses		mutUNG1 6244 n = 45 synapses	
	PSD length, nm	**Gold particles**	**PSD length, nm**	**Gold particles**	**PSD length, nm**	**Gold particles**
Average:	278.25	1.37	281.02	1.28	276.94	1.33
Standard deviation:	68.70	0.80	69.95	0.65	57.01	0.64
Average deviation:	54.47	0.55	53.06	0.45	45.42	0.49
Max:	428.40	5.00	479.14	4.00	409.64	4.00
Min:	145.66	1.00	139.28	1.00	153.23	1.00

Table A.2 A summary of the synapses analyzed in mutUNG1 expressing mice labeled with antibodies for GluA1.

	WT 6233 n = 42 synapses		WT 6234 n = 55 synapses		WT 6235 n = 50 synapses	
	PSD length, nm	**Gold particles**	**PSD length, nm**	**Gold particles**	**PSD length, nm**	**Gold particles**
Average:	258.20	3.37	252.87	2.83	247.40	3.02
Standard deviation:	65.15	2.48	60.95	1.72	61.32	1.86
Average deviation:	54.58	2.04	47.75	1.26	47.05	1.26
Max:	371.04	10.00	417.61	8.00	432.67	8.00
Min:	105.55	1.00	134.92	1.00	126.97	1.00

	WT 6236 n = 51 synapses		WT 6237 n = 54 synapses		WT 6238 n = 51 synapses	
	PSD length, nm	**Gold particles**	**PSD length, nm**	**Gold particles**	**PSD length, nm**	**Gold particles**
Average:	265.98	3.24	294.43	4.00	314.87	4.15
Standard deviation:	54.64	1.76	82.65	2.28	95.78	2.70
Average deviation:	45.67	1.43	66.14	1.90	77.80	2.05
Max:	365.58	7.00	487.84	9.00	579.69	14.00
Min:	148.07	1.00	144.67	1.00	159.22	1.00

Table A.3 A summary of the synapses analyzed in wild type mice labeled with antibodies for GluA2&3.

	mutUNG1 6239 n = 40 synapses		mutUNG1 6240 n = 47 synapses		mutUNG1 6241 n = 50 synapses	
	PSD length, nm	**Gold particles**	**PSD length, nm**	**Gold particles**	**PSD length, nm**	**Gold particles**
Average:	301.59	3.15	281.27	3.23	301.37	2.70
Standard deviation:	84.00	2.24	90.42	2.62	76.93	1.51
Average deviation:	68.30	1.90	79.41	1.93	62.14	1.35
Max:	474.51	7.00	443.65	13.00	485.97	5.00
Min:	170.48	1.00	108.78	1.00	149.25	1.00

	mutUNG1 6242		mutUNG1 6243 n = 45 synapses		mutUNG1 6244 n = 49 synapses	
	PSD length, nm	**Gold particles**	**PSD length, nm**	**Gold particles**	**PSD length, nm**	**Gold particles**
Average:	-	-	297.70	3.43	283.90	3.48
Standard deviation:	-	-	81.63	2.35	75.31	2.16
Average deviation:	-	-	65.33	1.91	57.18	1.72
Max:	-	-	469.71	10.00	485.47	8.00
Min:	-	-	145.19	1.00	153.40	1.00

Table A.4 A summary of the synapses analyzed in mutUNG1 expressing mice labeled with antibodies for GluA2&3. mutUNG1 6242 has no data because the section did not contain the CA1 area.

	WT 6233 n = 41 synapses		WT 6234 n = 51 synapses		WT 6235 n = 45 synapses	
	PSD length, nm	**Gold particles**	**PSD length, nm**	**Gold particles**	**PSD length, nm**	**Gold particles**
Average:	247.61	1.61	239.03	1.68	246.95	1.78
Standard deviation:	61.90	0.95	55.08	1.13	59.44	1.19
Average deviation:	50.02	0.68	43.14	0.77	46.77	0.80
Max:	396.76	6.00	416.64	7.00	411.88	7.00
Min:	133.53	1.00	134.22	1.00	112.12	1.00

	WT 6236 n = 46 synapses		WT 6237 n = 46 synapses		WT 6238 n=47 synapses	
	PSD length, nm	**Gold particles**	**PSD length, nm**	**Gold particles**	**PSD length, nm**	**Gold particles**
Average:	252.42	2.00	257.76	1.73	254.53	1.56
Standard deviation:	66.10	1.20	51.07	0.90	77.89	0.87
Average deviation:	53.73	0.83	40.79	0.71	57.68	0.74
Max:	382.42	6.00	382.33	4.00	500.16	4.00
Min:	130.44	1.00	176.32	1.00	144.27	1.00

Table A.5 A summary of the synapses analyzed in wild type mice labeled with antibodies for NR1.

	mutUNG1 6239 n = 47 synapses		mutUNG1 6240 n = 47 synapses		mutUNG1 6241 n = 47 synapses	
	PSD length, nm	**Gold particles**	**PSD length, nm**	**Gold particles**	**PSD length, nm**	**Gold particles**
Average:	268.25	1.59	249.18	2.07	249.90	1.34
Standard deviation:	69.07	0.71	76.32	1.35	82.37	0.69
Average deviation:	58.14	0.63	53.65	0.99	65.06	0.52
Max:	414.51	3.00	464.51	6.00	494.34	4.00
Min:	152.87	1.00	112.88	1.00	158.05	1.00

	mutUNG1 6242 n = 45 synapses		mutUNG1 6243 n = 47 synapses		mutUNG1 6244 n = 46 synapses	
	PSD length, nm	**Gold particles**	**PSD length, nm**	**Gold particles**	**PSD length, nm**	**Gold particles**
Average:	246.15	2.12	244.57	2.02	252.02	1.51
Standard deviation:	66.85	1.12	71.33	1.25	59.66	0.68
Average deviation:	48.74	0.81	56.28	0.96	49.49	0.57
Max:	474.79	6.00	455.38	6.00	371.77	4.00
Min:	142.74	1.00	126.58	1.00	142.93	1.00

Table A.6 A summary of the synapses analyzed in mutUNG1 expressing mice labeled with antibodies for NR1.

	WT 6233 n = 42 synapses		WT 6234 n = 49 synapses		WT 6235 n = 54 synapses	
	PSD length, nm	**Gold particles**	**PSD length, nm**	**Gold particles**	**PSD length, nm**	**Gold particles**
Average:	240.57	1.50	216.35	1.49	216.62	1.61
Standard deviation:	52.77	0.71	51.63	0.74	54.35	0.70
Average deviation:	38.19	0.60	38.91	0.62	40.90	0.62
Max:	405.58	4.00	389.43	4.00	364.38	3.00
Min:	158.22	1.00	131.65	1.00	139.70	1.00

	WT 6236 n = 44 synapses		WT 6237 n = 48 synapses		WT 6238 n = 47 synapses	
	PSD length, nm	**Gold particles**	**PSD length, nm**	**Gold particles**	**PSD length, nm**	**Gold particles**
Average:	229.28	1.41	212.94	1.50	236.52	1.50
Standard deviation:	67.08	0.69	43.51	0.82	71.03	0.66
Average deviation:	53.27	0.58	31.06	0.66	52.62	0.59
Max:	383.83	3.00	365.17	4.00	452.49	3.00
Min:	102.54	1.00	137.25	1.00	107.41	1.00

Table A.7 A summary of the synapses analyzed in wild type mice labeled with antibodies for NR2A&B.

	mutUNG1 6239 n = 48 synapses		mutUNG1 6240 n = 46 synapses		mutUNG1 6241 n = 51 synapses	
	PSD length, nm	**Gold particles**	**PSD length, nm**	**Gold particles**	**PSD length, nm**	**Gold particles**
Average:	224.36	1.43	215.02	1.45	253.27	1.61
Standard deviation:	63.49	0.70	56.49	0.66	69.36	1.02
Average deviation:	52.55	0.59	43.96	0.56	55.98	0.81
Max:	374.81	3.00	396.02	4.00	419.22	5.00
Min:	134.17	1.00	115.41	1.00	147.18	1.00

	mutUNG1 6242 n = 51 synapses		mutUNG1 6243 n = 50 synapses		mutUNG1 6244 n = 53 synapses	
	PSD length, nm	**Gold particles**	**PSD length, nm**	**Gold particles**	**PSD length, nm**	**Gold particles**
Average:	225.44	1.60	222.25	1.63	238.70	1.86
Standard deviation:	64.82	1.00	57.11	0.82	53.75	0.83
Average deviation:	51.78	0.73	41.80	0.70	40.92	0.64
Max:	431.51	6.00	369.61	4.00	404.64	4.00
Min:	134.51	1.00	117.33	1.00	149.69	1.00

Table A.8 A summary of the synapses analyzed in mutUNG1 expressing mice labeled with antibodies for NR2A&B.